Review

Prospects and Technical Challenges in Hydrogen Production through Dry Reforming of Methane

Fábio Gonçalves Macêdo de Medeiros [ID], Francisco Wendell Bezerra Lopes [ID] and Bruna Rego de Vasconcelos *[ID]

Biomass Technology Laboratory, Department of Chemical and Biotechnological Engineering,
Université de Sherbrooke, Sherbrooke, QC J1K 2R1, Canada;
fabio.goncalves.macedo.de.medeiros@usherbrooke.ca (F.G.M.d.M.);
francisco.wendell.bezerra.lopes@usherbrooke.ca (F.W.B.L.)
* Correspondence: bruna.rego.de.vasconcelos@usherbrooke.ca

Abstract: Environmental issues related to greenhouse gases (GHG) emissions have pushed the development of new technologies that will allow the economic production of low-carbon energy vectors, such as hydrogen (H_2), methane (CH_4) and liquid fuels. Dry reforming of methane (DRM) has gained increased attention since it uses CH_4 and carbon dioxide (CO_2), which are two main greenhouse gases (GHG), as feedstock for the production of syngas, which is a mixture of H_2 and carbon monoxide (CO) and can be used as a building block for the production of fuels. Since H_2 has been identified as a key enabler of the energy transition, a lot of studies have aimed to benefit from the environmental advantages of DRM and to use it as a pathway for a sustainable H_2 production. However, there are several challenges related to this process and to its use for H_2 production, such as catalyst deactivation and the low H_2/CO ratio of the syngas produced, which is usually below 1.0. This paper presents the recent advances in the catalyst development for H_2 production via DRM, the processes that could be combined with DRM to overcome these challenges and the current industrial processes using DRM. The objective is to assess in which conditions DRM could be used for H_2 production and the gaps in literature data preventing better evaluation of the environmental and economic potential of this process.

Keywords: dry reforming of methane; hydrogen production; catalyst development; industrial conditions; evaluation of environmental and economic potential
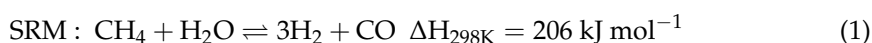
1. Introduction

The energy transition is currently one of the major global challenges and will require the development of various new technologies allowing the economical production of low-carbon energy vectors. Hydrogen (H_2) is an energy vector that can be used as a fuel or as raw material in the chemical industry and in the production of synthetic fuels (ammonia, synthetic CH_4, synthetic liquid fuels and methanol) [1]. Hence, due to its large use in high-emitting sectors such as transport and industry, H_2 (when produced in a sustainable way) can be a key enabler of the energy transition.

H_2 is currently produced from fossil fuels, biomass or water. Currently, steam reforming of methane (SRM, Equation (1)) is the main process used for the dedicated H_2 production [1]. However, the production of H_2 from fossil resources, such as natural gas or coal, is responsible for significant CO_2 emissions. According to the International Energy Agency (IEA), 10 tons of CO_2 are generated per ton of H_2 when it is produced from natural gas.

In order for H_2 to have a significant impact on the energy transition, it has to be produced in a sustainable way. Water electrolysis using renewable electricity is the main technology currently investigated since it produces high-purity H_2 from renewable energy and water. However, there are still some drawbacks related to high costs, technology

readiness level, renewable electricity supply and the coupling of electrolyzers with variable renewable energy depending on the type of electrolyzer used [2]. There are already a large number of reviews available in the open literature about H_2 production through water electrolysis [3,4]. Hence, this technology will not be discussed in the present paper. Another alternative technology that has been considered in the literature for H_2 production is dry reforming of methane (DRM, Equation (2)). This process allows the conversion of two major greenhouse gases (GHG) into a mixture of H_2 and carbon monoxide (CO) with a H_2/CO ratio of 1.

$$\text{SRM}: CH_4 + H_2O \rightleftharpoons 3H_2 + CO \quad \Delta H_{298K} = 206 \text{ kJ mol}^{-1} \tag{1}$$

$$\text{DRM}: CH_4 + CO_2 \rightleftharpoons 2H_2 + 2CO \quad \Delta H_{298K} = 247 \text{ kJ mol}^{-1} \tag{2}$$

However, there are issues preventing the use of this process at larger scale, especially for H_2 production. DRM is a highly endothermic reaction and both CH_4 and CO_2 conversion are favored at high temperatures, especially above 600 °C. Figure 1 presents the equilibrium concentrations as a function of temperature for all the species when DRM is operated at atmospheric pressure [5]. Several side reactions (Equations (3)–(6)) producing solid carbon and water are also possible and they not only lead to catalyst deactivation, but they also decrease the final H_2/CO of the syngas produced, which is a major issue when DRM is considered for H_2 production. For temperatures above 800 °C, reverse water gas shift (RWGS) reaction (Equation (6)) is especially favored, which reduces the H_2 production [6].

$$\text{Methane cracking}: CH_4 \rightleftharpoons C_{(s)} + 2H_2 \quad \Delta H_{298} = 75 \text{ kJ/mol} \tag{3}$$

$$\text{Boudouard reaction}: 2CO \rightleftharpoons CO_2 + C_{(s)} \quad \Delta H_{298} = -172 \text{ kJ/mol} \tag{4}$$

$$\text{Steam gasification of carbon}: C_{(s)} + H_2O \rightleftharpoons CO + H_2 \quad \Delta H_{298} = 131 \text{ kJ/mol} \tag{5}$$

$$\text{RWGS}: CO_2 + H_2 \rightleftharpoons H_2O + CO \quad \Delta H_{298} = 41 \text{ kJ/mol} \tag{6}$$
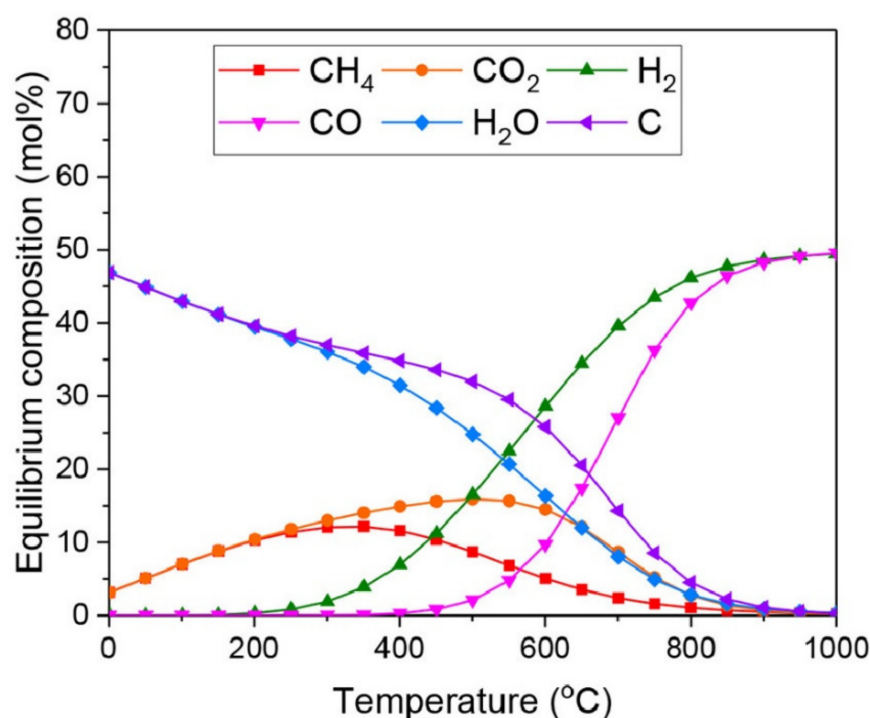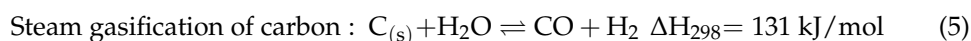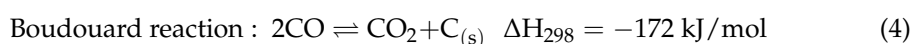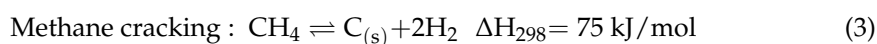

Figure 1. Thermodynamic equilibrium plot for DRM as a function of temperature (T = 0–1000 °C) at 1 bar and CH_4/CO_2 = 1. Reprinted from [5] in the terms of CC-BY license. Copyright 2022 [5].

Most of the recent DRM papers published in the literature are focused on catalyst development, especially on overcoming the constraints that lead to catalyst deactivation [7–12]. However, very few of them actually analyze the viability of this process for H_2 production [13]. The present paper aims to assess and present in which conditions DRM could be used as a viable pathway for H_2 production. The paper will first present the performance of the most recent DRM catalysts developed for producing syngas with high H_2/CO. Then, it will present other reforming technologies currently investigated that could eventually be combined with DRM to increase the syngas' H_2/CO ratio. This part will be followed by pilot and commercial scale DRM process reported in the literature as well as the goals of these processes. Finally, based on these findings, an outlook will be presented highlighting the viability of this process for H_2 production based on the current findings and what it would take for its economic viability.

2. Recent Advances on Catalysts for Syngas Production

There are already numerous reports in the literature on the development of new catalysts for DRM to overcome catalyst deactivation via coking and sintering of support and active phase as well as to decrease the cost effectiveness of the overall catalytic system. Hence, these aspects will not be discussed in this work. The focus of the present section will be to identify the catalysts able to produce syngas with high H_2/CO, aiming at H_2 production as well as the process conditions required to achieve this ratio.

2.1. Noble Metal-Based Catalysts

The catalytic activity of noble metals from groups VIII to X (Ru, Rh, Ir, Pd, Pt) has been thoroughly investigated towards DRM when supported over different materials. These noble metals present high catalytic activity for CH_4 and CO_2 conversion (X_{CH_4} and X_{CO_2}, respectively) and distinct stability against thermal and oxidative sintering and, especially, coke deposition [14,15]. The observed activity of noble metals for DRM follow the order Rh > Ru > Ir > Pt > Pd [16]. Nonetheless, the use of noble metals for such purpose still present, as major drawbacks, the low abundance, high costs and usual toxicity [17]. Recently, research has focused not only on highly active catalysts using noble metals at low concentrations (Table 1), which has been proven effective, but also on the promoting effects of noble metals for transition metal-based catalysts, aiming to enhance their resistance against coke deposition [18,19].

Ruthenium is one of the cheapest noble metals (still almost 500 times more expensive than nickel) that presents a good catalytic performance for DRM [16]. Andraos et al. [20] explored the effect of different supports (Al_2O_3, $MgAl_2O_4$ and YSZ) on the DRM activity of mono- (Ru) and bimetallic (Ru, Ni) catalysts for hydrogen production. Despite the high catalyst activity of monometallic Ru/Al_2O_3 catalyst (T = 750 °C, X_{CH_4} = 90%, X_{CO_2} = 93%, H_2/CO = 0.94), the highest hydrogen production was obtained when 5 wt% Ni/Al_2O_3 catalyst was promoted with 1 wt% Ru (T = 750 °C, X_{CH_4} = 94%, X_{CO_2} = 97%, H_2/CO = 0.97). Ru functionalization also increased the overall catalyst stability by preventing catalyst sintering and the formation of poorly active phases, such as $NiAl_2O_4$ for the $Ru-Ni/Al_2O_3$ catalyst. On the other hand, poor metal dispersion after Ru promotion (maximum dispersion of 6%) was responsible for an increase in carbon deposition over the Ni-based catalyst (from 0.18% to 0.32% for Ni/Al_2O_3 and $Ru-Ni/Al_2O_3$, respectively) [20]. A high metal dispersion was found to promote a stronger interaction between Ru particles and the catalyst support and lead to lower carbon deposition and increased catalyst stability [21].

Anil et al. [22] investigated the performance of partially substituted perovskites $LaAlO_3$ by 2 wt% of noble metals Ru, Pt and Pd for the DRM reaction at 800 °C. The authors reported that Ru-substituted $LaAl_{0.98}Ru_{0.02}O_{3-\delta}$ presented the highest hydrogen production, reaching a H_2/CO ratio 0.85 with CH_4 and CO_2 conversions of 86% and 100%, respectively. Strong occurrence of RWGS reaction along with DRM was responsible for straying the H_2/CO from unity in all cases, especially on the Pt-substituted

$LaAl_{0.98}Pt_{0.02}O_{3-\delta}$ ($H_2/CO = 0.60$). Moreover, on the stability study at 650 °C for 50 h, no significant efficiency reduction was observed on the $LaAl_{0.98}Ru_{0.02}O_{3-\delta}$.

Rhodium has also been evaluated as an effective noble metal with distinct catalytic activity towards DRM [16]. In the study of Moreira et al. [23], the performance of the 0.1 wt% Rh/Al_2O_3 catalyst was compared with 10 wt% Ni/Al_2O_3. The authors reported that, when incipient wetness impregnation method was used for catalyst preparation, the Rh-based catalyst presented a higher S_{BET} (191.8 m^2 g^{-1}) and a much higher metal dispersion (45.1%) when compared to the 10 wt% Ni/Al_2O_3 catalyst (154.3 m^2 g^{-1} and 1.9%, respectively). The catalytic tests at 700 °C showed that the hydrogen selectivity over the 0.1 wt% Rh/Al_2O_3 was slightly higher, leading to a H_2/CO ratio of 0.91, while the 10 wt% Ni/Al_2O_3 presented a H_2/CO ratio of 0.89 under the same test conditions. However, stability tests at 700 °C showed that the 0.1 wt% Rh/Al_2O_3 catalyst performed up to 184 h of time on stream (TOS) with H_2/CO ratio higher than 0.95, CH_4 conversion of 65% and CO_2 conversion of 58% with no signs of deactivation. On the other hand, the 10 wt% Ni/Al_2O_3 catalyst showed a strong deactivation trend due to sintering and coke deposition at 24–70 h, with significant decrease in the H_2/CO ratio to 0.80.

Platinum is a specially studied noble metal for DRM [24–26]. Among the optimization goals on Pt-based catalysts, metal dispersion, size and, especially, phase of Pt particles (with ionic Pt^{2+} presenting higher DRM activity than metallic Pt^0) have demonstrated a great deal of influence on the catalytic performance [27]. Carvalho et al. [28] evaluated the deposition of Pt over mesoporous alumina promoted with metal oxides (MgO, ZrO_2, CeO_2 and La_2O_3) and reported good stability under DRM conditions. On this study, the authors reported that the Pt/CeO_2-Al_2O_3 catalysts presented the highest activity for DRM at 700 °C with CH_4 and CO_2 conversions of 90% and 78%, respectively, and a high H_2/CO of 0.90. The authors hypothesize that a combination of CH_4 cracking and reverse Boudouard reaction may have compromised the H_2 production over the other oxide-modified catalysts. Moreover, this catalytic performance was maintained for over 24 h even though coke deposition had taken place.

The resistance of Pt against coke deposition as a main trigger for catalyst deactivation was also reported by Xie et al. [29]. The authors evaluated the addition of Pt to CeO_2-supported cobalt catalysts in order to describe a possible synergistic effect on the bimetallic catalyst responsible for an activity boost. Kinetic and density-functional theory (DFT) calculations revealed that the CO_2 is much more easily activated over the PtCo surface (69 $kJ.mol^{-1}$) when compared to the monometallic surfaces. In addition, the authors also reported that the enhanced presence of oxygen radicals on the support surface due to the oxygen storage capacity (OSC) of CeO_2 also favored the activation of CH_4 via oxygen-assisted activation pathway ($CH_4^* + O^* \rightarrow CH_3^* + OH^*$). Furthermore, the authors reported that the Co/CeO_2 catalyst presented low activity on higher temperatures (>600 °C), which yielded the lowest H_2/CO ratio of 0.3. On the other hand, the Pt/CeO_2 and $PtCo/CeO_2$ catalysts presented around 95% conversion of both CH_4 and CO_2 at 750 °C with H_2/CO higher than 0.95.

Table 1. Summary of catalytic systems recently reported for H_2 production via DRM.

Catalyst	Preparation Method	Reaction Conditions	X_{CH_4} (%)	X_{CO_2} (%)	H_2/CO Ratio	Coke Deposition	Ref.
		Noble metal-based catalysts					
0.1 wt% Rh- and 10 wt% Ni-based catalysts supported on γ-Al_2O_3	Incipient wetness impregnation	700–800 °C, CH_4:CO_2 = 1:1; GHSV = 12–108 h^{-1}	92	98	>0.97	nr	[23]
2 wt% Ru-, Pt- and Pd-substituted $LaAlO_3$	Combustion synthesis	400–800 °C, CH_4:CO_2:N_2 = 0.1:0.1:0.8, GHSV = 48,000 h^{-1}	>60	>80	0.6–0.85	nr	[22]

Table 1. *Cont.*

Catalyst	Preparation Method	Reaction Conditions	X_{CH_4} (%)	X_{CO_2} (%)	H_2/CO Ratio	Coke Deposition	Ref.
0.16 wt% Pt-CeZrO$_2$ supported on carbon fibers	Co-precipitation	800 °C, CH$_4$:CO$_2$:Ar = 0.04:0.1:0.86, GHSV = 5000 h^{-1}	40	52	0.30	nr	[30]
Core-shell 0.6 wt%Ru@SiO$_2$	Reverse-phase microemulsion	700 °C, CH$_4$:CO$_2$:N$_2$ = 1:1:1, WHSV = 34.8 L h^{-1} g^{-1}	68	70	0.90	nr	[31]
Nickel-based catalysts							
10 wt%Ni/MgAl$_2$O$_4$	Microwave-assisted combustion	800 °C, CH$_4$:CO$_2$:N$_2$ = 0.1:0.1:0.8, WHSV = 72 L h^{-1} g^{-1}	>75	>80	>0.90	2–6 wt%	[32]
1–5 wt% K-promoted 10 wt%Ni/Al$_2$O$_4$	Co-precipitation	650 °C, CH$_4$:CO$_2$:N$_2$ = 0.2:0.2:0.6, WHSV = 30 L h^{-1} g^{-1}	35–55	42–58	0.50–0.86	No coke for 5 wt% K promotion	[33]
1–8 wt% Mn-promoted 3–8 wt% Ni/Al$_2$O$_3$	Wet impregnation	750 °C, CH$_4$:CO$_2$:Ar = 1:1:1, WHSV = 36 L h^{-1} g^{-1}	70–80	80–90	0.70–0.76	nr	[34]
Mg(Ni)Al$_2$O$_4$ spinel	Co-precipitation	850 °C, CH$_4$:CO$_2$:N$_2$ = 30:80:90, WHSV = 120 L h^{-1} g^{-1}	90	98	1.4	nr	[35]
10 wt% Ni/Al$_2$O$_3$	Microwave-assisted combustion	700 °C, CH$_4$:CO$_2$:N$_2$ = 0.1:0.1:0.8, WHSV = 72 L h^{-1} g^{-1}	72–87	72–87	1.09	13.7 wt%	[36]
1–2 wt% Fe promoted 5–15 wt% Ni/MgAl$_2$O$_4$ catalyst	Incipient wetness impregnation	650–850 °C, CH$_4$:CO$_2$ = 1:1, WHSV = 30,000 L g^{-1} h^{-1}	57–100	62–95	0.82–1.01	2.1–34.2 wt%	[37]
10 wt% Mo promoted 10 wt% Ni/Al$_2$O$_3$ catalyst	Wet impregnation	550–850 °C, CH$_4$:CO$_2$ = 1:1, GHSV = 20,000 h^{-1}	6–91	8–93	0.40–0.93	nr	[38]
5 wt% La, Ce and Zr promoted 25 wt% Ni/Al$_2$O$_3$	Ultrasound assisted co-precipitation	550–700 °C, CH$_4$:CO$_2$ = 1:1, WHSV = 12,000 mL h^{-1} g^{-1}	0–70	40–80	0.6–1.1	nr	[39]
4.5 wt% Ni yolk-shell catalyst on hollow silica spheres (HSS)	Micro-emulsion impregnation	800 °C, CH$_4$:CO$_2$ = 1:1, WHSV = 36,000 mL h^{-1} g^{-1}	94	98	0.95	No coke	[40]
6.5 wt% Ni core-shell catalyst on 3 wt% ZrO$_2$/SiO$_2$	Micro-emulsion impregnation	550–800 °C, CH$_4$:CO$_2$ = 1:1, Flow rate = 15 mL min^{-1}	85–93	90–95	0.9–1.0	No coke	[41]
DMS-supported 7 wt% Ni nanoparticles	Ethylene glycol impregnation	700 °C, CH$_4$:CO$_2$ = 1:1, WHSV = 18 L h^{-1} g^{-1}	76	83	0.9	nr	[42]
Sandwiched SiO$_2$@8.9wt%Ni@ZrO$_2$ catalyst	Organic wet synthesis	500–900 °C, CH$_4$:CO$_2$ = 1:1, WHSV = 180 L h^{-1} g^{-1}	7–98	7–95	0.5–1.0	0–19 mg g$_{cat}^{-1}$ h^{-1}	[43]
5 wt% Ni supported on CeO$_2$-SiO$_2$	Incipient wetness impregnation	600–800 °C, CH$_4$:CO$_2$ = 1:1, WHSV = 48 L h^{-1} g^{-1}	66–97	51–92	0.77–0.94	nr	[44]
1–5 mol% Ce and Ca promoted Ni/MSC catalyst	Co-impregnation	650–900 °C, CH$_4$:CO$_2$ = 1:1, Flow rate = 120 mL min^{-1}	45–97	54–97	0.8–1.0	nr	[45]
3 wt% Sc, Y, Ce and Pr promoted 15wt% NiMgAl catalysts	Co-precipitation	750 °C, CH$_4$:CO$_2$ = 1:1, Flow rate = 45 mL min-1, WHSV = 15 L g^{-1} h^{-1}	86–88	95–96	0.97–0.98	nr	[46]
Cobalt-based catalysts							
10–25 mol% Co/MgO catalyst	Sol-gel method	750 °C, CH$_4$:CO$_2$ = 1:1, WHSV = 24 L h^{-1} g^{-1}	85–90	80–85	0.93–0.95	0–0.22 mg g$_{cat}^{-1}$ h^{-1}	[47]
0.1–2 wt% Ce-promoted 10 wt%Co/Al$_2$O$_3$	Incipient wetness impregnation	650–750 °C, CH$_4$:CO$_2$:N$_2$ = 0.2:0.2:0.6, WHSV = 36 L h^{-1} g^{-1}	75–82	63–72	0.86–0.91	7.5–12.8 wt%	[48]
3 wt%, Y, La, Ce or Sm-promoted 10 wt%Co/MA	Incipient wetness impregnation	750 °C, CH$_4$:CO$_2$:N$_2$ = 1:1:3.1, WHSV = 36 L h^{-1} g^{-1}	71–84	73–90	0.86–0.96	7–28 wt%	[49]
3 wt% La-promoted 10 wt% Co/Al$_2$O$_3$	Hydrothermal synthesis	750 °C, CH$_4$:CO$_2$ = 1:1, WHSV = 36 L h^{-1} g^{-1}	76–96	81–93	0.89–0.99	26–38 wt%	[50]
0.2–0.5 wt% Rd-promoted12 wt% Co/SBA-15	Two-solvent impregnation	550 °C, CH$_4$:CO$_2$ = 1:1, WHSV = 67 L h^{-1} g^{-1}	15–49	18–43	0.5–1.1	nr	[51]
0.5–2 wt% Sc-promoted 5 wt% Co/TiO$_2$	Incipient wetness impregnation	700 °C, CH$_4$:CO$_2$:N$_2$ = 17:17:2, WHSV = 3.6 L h^{-1} g^{-1}	82–84	82–85	0.94–0.96	6.8–32.3 wt%	[52]

Table 1. *Cont.*

Catalyst	Preparation Method	Reaction Conditions	X_{CH_4} (%)	X_{CO_2} (%)	H_2/CO Ratio	Coke Deposition	Ref.
		Other transition metal-based catalysts					
$LaNi_{0.34}Co_{0.33}Mn_{0.33}O_3$ perovskite catalyst	Microwave-assisted Pechini method	800 °C, CH_4:CO_2 = 1:1.05, WHSV = 12 L h^{-1} g^{-1}	94	93	1.1–1.2	nr	[53]
$LaNiO_3$ perovskite	One-step sol-gel method with chitosan	600–800 °C, CH_4:CO_2 = 1:1, WHSV = 6–24 L h^{-1} g^{-1}	48–95	45–95	0.65–1.25	16–34 wt%	[54]
$SmCoO_3$ perovskite	Sol-gel citrate method	700–800 °C, CH_4:CO_2 = 1:1, WHSV = 30 L h^{-1} g^{-1}	88–93	89–93	0.8–1.1	nr	[55]
		Bi-and trimetallic catalysts					
3–15 wt% Ce promoted 1 wt%Pt-1 wt%Pd-1 wt%Ni/MgO trimetallic	Co-precipitation	700–900 °C, CH_4:CO_2 = 1:1 and 2:1, Flow rate = 30 mL min^{-1}	60–83	39–98	0.4–1.1	2.4 wt%	[56]
0.1–0.5 wt% Rh-4.5–4.9 wt% Co/Al_2O_3	Wet co-impregnation	600–700 °C, CH_4:CO_2 = 1:1, GHSV = 1000–2000 h^{-1}	87–94	86–91	0.99–1.0	No coke	[57]
10.5 wt%Ni-4.5 wt%Co supported on Al_2O_3-MgO catalysts	Sol-gel method	800 °C, CH_4:CO_2 = 1:1, Flow rate = 40 mL min^{-1}	79	84	0.85–0.90	nr	[58]
$Co_2Ni_2Mg_2Al_2$ mixed oxide catalyst	Hydrotalcite route synthesis	500–800 °C, CH_4:CO_2 = 1:1, GHSV = 32,000 h^{-1}	97	91–93	0.8	nr	[59]
12.5 wt% Ni and 12.5 wt%Ni-2 wt%Co supported on CeO_2-$ZnAl_2O_4$	Co-precipitation	700 °C, CH_4:CO_2 = 1:1, WHSV = 180 L h^{-1} g^{-1}	76	88	0.99	38 wt%	[60]
7 wt% Ni and 7 wt%Ni-1 wt%Ru supported on SiO_2, ZrO_2, Al_2O_3 and $MgAl_2O_4$	Wet impregnation and precipitation	800 °C, CH_4:CO_2 = 1:1, Flow rate = 400 mL min^{-1}	39–100	48–85	0.5–1.0	0.1–0.42 wt%	[61]

nr—not reported; WHSV—weight hourly space velocity; GHSV—gas hourly space velocity; DMS—dendritic mesoporous silica; MSC—mesoporous silica-carbon; MA—mesoporous alumina; SBA-15—mesoporous silica.

2.2. Transition Metals-Based Catalysts

Transition metals from the groups VII to X, especially Co and Ni, have demonstrated good catalytic performance for DRM (Table 1). Due to their high catalytic performance and low cost when compared to noble metals, they have been considered as the way to go on improving DRM towards industrial hydrogen production [15,16]. However, the resistance of Ni- and Co-based catalysts against sintering and deactivation by coke deposition is much lower when compared to noble metals [18]. In this sense, several studies have been focused on improving synthesis methods, catalyst support and metal-support interactions in order to increase both the activity, hydrogen selectivity and the stability of transition metal-based catalysts [62].

2.2.1. Nickel Catalysts

Nickel-based catalysts have been extensively reported as highly active for DRM, with a catalytic activity comparable to iridium (a noble metal with higher DRM than Pt and Pd) [63]. Comprehensive studies have shown that the general bi-functional mechanism of DRM goes through a CH_4 dehydrogenation over non-valent metal sites, while basic sites on supports and promoters are responsible for CO_2 dissociation [64]. It has been reported that Ni active sites may present a favorable electron structure for favoring the activation and cleavage of the C–H bonds, which is an important mechanism step for CH_4 activation and H_2 production [65,66].

Chein et al. [67] investigated hydrogen production over 10 wt% Ni/Al_2O_3 with CeO_2 modification to better understand the role of feed composition and CeO_2–Al_2O_3 interaction on the activity and stability of Ni-based catalysts. The authors reported around 75% conversion of CH_4 and CO_2 at 800 °C, over 10 wt% Ni/Al_2O_3 catalysts with a H_2/CO ratio of 0.90. Adding up to 5 wt% CeO_2 to the alumina support led to an increase in both CH_4 and CO_2 conversion to 85% and 90%, respectively. Moreover, H_2 selectivity also increased, leading to a syngas with a H_2/CO of 0.93. Increasing CeO_2 loading from 5 to 15 wt% led to the reduction in the surface area from 104.5 to 90.5 m^2 g^{-1}, increased the probability of Ni particles' agglomeration and decreased the catalyst activity. Regarding feed composition,

the authors reported that CH_4 conversion increased when feed composition changed from $CH_4:CO_2 = 1:1$ to 1:3. However, this increase was not followed by a higher H_2 production, and the overall best H_2/CO ratio (0.90) was achieved at $CH_4:CO_2 = 1:1$. This observation points to the favoring of parallel reactions on higher $CH_4:CO_2$ ratios.

Ceria (CeO_2) promotion was also found favorable for H_2 production in a recent study by Farooqi et al. [11]. The authors evaluated the effects of La_2O_3 and CeO_2 promotions on 10 wt% Ni/Al_2O_3 catalysts synthesized by the sol-gel method. The authors reported that La-promotion may present a dual role on DRM catalysts by increasing their resistance to coke as well as decreasing the acidic character of the support. However, CeO_2 promotion was more advantageous when compared to La_2O_3 promotion when H_2/CO was considered. CeO_2 promotion led to a syngas with a H_2/CO ratio of 0.95, while a H_2/CO ratio of 0.89 was obtained when La_2O_3 was used as a promoter in the same test conditions. The authors highlighted that the presence of the CeO_2 improved the active phase dispersion and reducibility, which led to higher H_2/CO on the produced syngas.

Cruz-Flores et al. [68] evaluated the impact of a direct synthesis method via Ni-phyllosilicates for the production of $Ni-SiO_2$ catalysts in comparison to the incipient wetness impregnation method on the catalytic activity and stability of Ni-based catalysts on DRM. The authors reported that the $Ni-SiO_2$ catalysts synthesized via Ni-phyllosilicates presented a higher metal dispersion even for high Ni loadings (15 wt% Ni), which led to a reduced carbon formation on short reaction times. However, for longer reaction times (TOS > 180 min), significant carbon formation was observed in the temperature range of 600–900 °C. The results indicate that for T < 700 °C, the Boudouard reaction was favored, leading to a high carbon deposition. For T = 800–900 °C, the high H_2 yields (above 90%) were followed by H_2/CO ratio > 1.0 and high carbon formation, indicating the occurrence of CH_4 cracking and CO disproportionation reactions.

Mahfouz et al. [69] used KIT-6 mesoporous silica as support for Ni catalysts synthesis via wet impregnation and reported a high surface area of $S_{BET} = 422$ m^2 g^{-1} for the 15 wt% Ni/KIT-6 catalyst. The catalytic tests at T = 800 °C showed CH_4 and CO_2 conversions of 88% and 90%, respectively, and the production of syngas with a H_2/CO ratio of 0.92. Moreover, the authors evaluated that, although cerium promotion (ceria/KIT-6 ratio = 3/2) on the 15 wt% Ni/KIT-6 showed a slight increase on CH_4 and CO_2 conversion, the H_2/CO ratio at higher temperatures (>700 °C) was not altered. Furthermore, Mourhly et al. [70] have recently reported the synthesis of Ni-based catalysts over nano-sized mesoporous silica (MSN) as an alternative support. The MSN was prepared by alkaline leaching of silica-rich pumice rock. Different Ni loadings varying between 5 and 20 wt% were added to the MSN support by wet impregnation and tested in DRM at 550–750 °C. This study showed that increasing the amount of Ni on the catalysts did not improve CH_4 conversion due to the formation of Ni particles clusters with non-reactive aspects for hydrogen production. On the other hand, low Ni loading (5–10 wt%) led to high metal dispersion and strong metal-support interaction, favoring H_2 yields close to 70%.

One-pot microwave-assisted combustion synthesis was reported to be a fast and cost-effective method for producing high H_2-yielding 10 wt% Ni/Al_2O_3 catalysts by Medeiros et al. [71]. The authors showed that a low fuel/oxidant ratio for the combustion-based synthesis resulted in catalysts with high surface area ($S_{BET} = 266$ m^2 g^{-1}) and high reducibility (degree of reduction = 93%). Moreover, the microwave-synthesized 10 wt% Ni/Al_2O_3 catalysts presented an H_2 yield of 58% with low coke deposition (1.2 wt%) and H_2/CO ratio close to 1.0 over 20 h of TOS. The same research group has also reported microwave-assisted synthesis of alumina supports for DRM [36]. The synthesized alumina presented a high surface area (221.2 m^2/g) and was used as support for the deposition of 10 wt% Ni via incipient wetness impregnation for DRM evaluation. The catalyst presented significant DRM activity, with over 87% CO_2 conversion (T = 700 °C, GHSV = 72 L g^{-1} h^{-1}) at a 20 h test. The authors also report the production of a syngas with $H_2/CO = 1.09$ and 13.7 wt% carbon deposition.

Miri et al. [72] recently investigated the influence of several promoters (Fe, La, Zr, Ce and Ca) on the catalytic performance of 10 wt% Ni/MgAl$_2$O$_4$ for DRM and reported that La, Zr, Ce and Ca were able to improve Ni dispersion over the catalyst, which could increase catalytic activity. Furthermore, Ce was found to be the promoter which better increased CH$_4$ conversion (X$_{CH_4}$ = 48%), at an optimal loading of 3 wt% Ce. Finally, the authors evaluated that the overall H$_2$/CO ratio could be tuned as a function of CH$_4$/CO$_2$ feed composition, and the highest H$_2$/CO = 1.4 was obtained at CH$_4$/CO$_2$ = 2.0.

2.2.2. Cobalt Catalysts

Along with nickel and its applications as DRM catalysts, cobalt has also been investigated as an alternative, inexpensive and earth-abundant metal with distinct catalytic activities for CH$_4$ reforming [73,74]. However, cobalt-based catalysts have similar deactivation issues as those observed with nickel catalysts. Studies have shown that coke deposition is also a major trigger for Co-based catalysts deactivation, along with active sites oxidation [47,75,76]. Mechanistic studies via DFT showed that the metal-support interaction, metal distribution (related to the metal particle size) and active site oxidation stage play a significant role on the reaction rates for H$_2$ production and on the deactivation of cobalt sites during DRM. [77].

The influence of cobalt loading on sol-gel synthesized Co/MgO catalysts was investigated by Sukri et al. [47] with focus on the carbon deposition over the cobalt sites. The authors evaluated Co-loadings from 10 wt% to 25 wt% and reported an increase in the number of active sites at higher Co loads (20–25 wt%). On the other hand, the active phase at higher Co loads presented a weaker interaction with the catalyst support which led to a higher rate of carbon deposition. The similar catalytic activity shown by all evaluated catalysts showed a saturation behavior on the loading increase in Co. Furthermore, the authors evaluated the stability of 10 wt% Co/MgO catalyst for 50 h at 750 °C and reported the production of syngas with a H$_2$/CO ratio of 0.94 along with high CH$_4$ and CO$_2$ conversions of 82% and 88%, respectively, and a low carbon formation rate (0.0072 g g$_{cat}$$^{-1}$ h^{-1}). Al Abdulghani et al. [78] investigated the promotion of ZrO$_2$-supported Co catalysts with boron (B) for increasing reactivity towards CH$_4$ and CO$_2$ conversion. The authors showed that B impurities interacted with Co particles on the catalyst and increased hydrogen production as a result of increased reactivity of the Co/ZrO$_2$ catalyst by three times towards CH$_4$ decomposition.

Ayodele et al. [79] investigated the influence of CH$_4$:CO$_2$ feed ratio from 0.1 to 1.0 on the DRM activity of CeO$_2$-supported Co catalysts synthesized with 20 wt% Co by incipient wetness impregnation. The authors also reported that the highest CH$_4$ (75–80%) and CO$_2$ (80–90%) conversions were obtained for a temperature of 750 °C. The final H$_2$/CO ratio reached was 0.98–1.0 when the feed ratio (CH$_4$:CO$_2$) varied between 0.8 and 0.9. Moreover, although no activity loss was observed during the tests, TEM images of spent catalysts showed that the particle size of active sites increased, which could, in turn, lead to sintering and irreversible deactivation.

Tran et al. [80] evaluated a novel filament-shaped mesoporous γ-Al$_2$O$_3$ as catalyst support for 10 wt%Co nanoparticles and reported an increase in H$_2$ production when compared to commercial γ-Al$_2$O$_3$ support. The authors reported that the highest CH$_4$ (76%) and CO$_2$ (82%) conversion was obtained at 800 °C and the H$_2$/CO ratio increase from 0.83 to 0.89 when comparing the commercial as synthesized γ-Al$_2$O$_3$ supports, respectively. On the other hand, the authors highlight that such H$_2$/CO increase was a result of CH$_4$ cracking reaction (Equation (3)), which resulted in a higher carbon deposition (47 wt%) for the synthesized alumina support.

Tungsten carbide (WC) has been referred to in literature as presenting activity comparable to noble metals and a "Pt-like" behavior for CO$_2$ conversion [81], which has motivated recent studies on its application [82,83]. Li et al. [84] have evaluated the DRM activity of 13 wt% Co-based catalysts supported on activated carbon-modified WC (WC-AC) and reported high stability of the prepared catalysts. According to the authors, at 800 °C, both

CH_4 and CO_2 conversions were maintained over 90% for a 50 h test with minor activity drop, while H_2/CO ranged from 0.90 to 0.92 during the whole test. The authors evaluated that an optimal 6.5 wt% W loading on the support was responsible for decreasing the activation energy of the reactants and boosted the catalytic activity. Furthermore, Wang et al. [85] also evaluated the activity of the Co/WC-AC catalyst and reported the effects of La-promotion. Although no significant improvement on H_2/CO ratio was observed, the authors showed that a 10–20 wt% La addition to the catalyst could prevent catalyst sintering and the formation of poorly active $CoWO_4$ phase on the support, which could lead to catalyst deactivation.

2.2.3. Other Transition Metals

Ni and Co are the most investigated metals for their known and vastly reported catalytic activities towards DRM. However, recent studies have also investigated other transition metals and their role on the catalyst development process for a successful scaling up of DRM process. Dehimi et al. [86] evaluated the effect of temperature on the catalytic activity of Mo-based catalysts doped with Ni on DRM. The catalysts were prepared by incipient wetness impregnation with a nominal load of 20 wt% Mo and a variable load (2–10 wt%) of Ni. The authors reported that the increase in Ni loading to 10 wt% was responsible for a higher Mo dispersion over the catalyst support (Al_2O_3), which positively affected CH_4 and CO_2 conversion. However, the authors highlighted that although the high Mo loading may have been responsible for a low conversion at T = 800 °C (X_{CH_4} = 30%, X_{CO_2} = 48%, H_2/CO = 0.40), the Mo-based catalysts presented no coke deposition after the catalytic tests, which may lead to a higher catalyst stability.

Vroulias et al. [87] has recently reported the investigation on the effect of W loading on Ni/Al_2O_3 catalysts for DRM. The catalysts prepared by wet co-impregnation had a W-loading ranging from 0 to 26.2 wt% of W and were tested for DRM at 700 °C. The highest concentrations of W on the catalysts (19.8 wt% and 26.2 wt%) inhibited DRM activity (X_{CH_4} < 20%) and the best results were achieved with intermediate W loadings (6.3 wt% and 11.9 wt%; T = 700 °C, X_{CH_4} = 55–60%, X_{CO_2} = 60–70%). These loadings, however, led to the production of syngas with a low H_2/CO ratio of 0.5–0.8. Finally, the authors reported that the presence of W was responsible for suppressing coke formation due to a double mechanism: the restrained carbon diffusion on the lattice of Ni-W alloys, and the carbon formation-gasification mechanism that took place on the surface of the catalysts and yielded the formation of tungsten carbides.

2.2.4. Bi- and Trimetallic Catalysts

Bi- and trimetallic catalysts have been widely explored for DRM (Table 1). Studies have shown that the presence of more than one metal on the catalyst may result in a synergistic effect, with all metals acting as active phases or, by a promotion effect, when the active metal has its intrinsic activity enhanced by the presence of a second/third doping metal. Such synergistic effects could be explained by the electronic modifications on the catalyst surface as a result of the presence of a second/third metal, which could translate as increasing reactants chemisorption, for example [88]. Those effects can range from the stabilization of metal particles to improvements in metal-support interactions, metal dispersion and reducibility [89,90]. Increased metal dispersion and strong metal-support interactions, for example, have already been linked to performance improvements on DRM, such as higher H_2 yields and suppressing of coke formation [91]. Furthermore, recent DFT modeling and calculations have considered that the appropriate fine-tuning active phase composition can lead to the suppressing of DRM side reactions, such as RWGS, which would contribute to higher H_2/CO ratio on the final syngas [92].

Al-Fatesh et al. [93] evaluated the effect of calcination temperature and reduction protocols on the DRM activity of Ni-Co bimetallic catalysts supported on Al_2O_3-ZrO_2 mixed oxide. The catalysts were prepared by co-precipitation and subjected to different in situ and ex situ calcination and reduction protocols before being tested on DRM reaction at

500–800 °C. The authors demonstrated that the catalysts calcined at 800 °C and reduced in situ prior to catalytic evaluation at 700 °C yielded the best performance, with CH_4 and CO_2 conversions of 67% and 76%, respectively, and a H_2/CO ratio of 0.91. The authors reported that the calcination at a high temperature triggered sintering and particle growth to a degree that increased both catalytic activity and stability. Bimetallic Ni-Co catalysts were also investigated by Movasati et al. [60]. The catalysts were prepared by co-impregnation using CeO_2-$ZnAl_2O_4$ mixed oxide as support. In this study, the authors reported that the presence of cobalt increased the catalyst's surface area when compared to Ni monometallic catalysts from 39.87 $m^2\,g^{-1}$ to 46.27 $m^2\,g^{-1}$. The number of basic sites also increased from 180.3 $\mu mol\,g^{-1}$ to 190.1 $\mu mol\,g^{-1}$ when Co was added as a promoter. The metal-support interaction was also favored and prevented the sintering of the active phase. Finally, Ni-Co/CeO_2-$ZnAl_2O_4$ catalyst yielded a CH_4 and CO_2 conversion of 76% and 88% at T = 700 °C, respectively, with a high H_2/CO ratio of 0.99.

Turap et al. [94] investigated different Co/Ni ratios on the preparation of CeO_2-supported Co-Ni catalysts for DRM application. The authors prepared a series of bimetallic catalysts by co-impregnation with Co/Ni ratios of 0.3–1.0 with a fixed 10 wt% Ni content and evaluated the catalytic activity for DRM between 600 and 850 °C. Reducibility studies showed that at the ratio of 0.8 Co/Ni, the Co addition improved catalyst reduction capacity, increased the metal-support interaction, when compared to Co- and Ni-based monometallic catalysts, and changed the configuration of bulk oxygen from CeO_2 support. In addition, the 0.8Co–Ni/CeO_2 catalyst presented the best catalytic performance at 850 °C, reaching CH_4 and CO_2 conversions of 99% and 100%, respectively, and a H_2/CO ratio of 0.98.

Trimetallic NiFeCu alloys with a Ni/Fe = 3.0 and different amounts of Cu were prepared by co-precipitation and investigated as a catalyst for hydrogen production via DRM in a recent work by Jin et al. [95]. The catalytic performance tests showed that the excess addition of Cu (Cu/Fe = 1.5) results in a decreased initial activity for CH_4 and CO_2 conversion and severe deactivation by carbon deposition (12.7 wt%), due to possible coverage of Ni active sites by Cu. Overall, the Cu addition in the ratio of Cu/Fe = 0.5 delivered the highest H_2/CO = 0.60 at T = 750 °C with a CH_4 conversion of 50%. H_2 production of the trimetallic catalyst was comparable to the bimetallic NiFe catalysts, but the presence of Cu increased the amount of oxygen species on the catalyst surface and decreased carbon deposition by 50%.

2.2.5. Role of Catalyst Support

Although studies have stated that the catalyst support itself would not take part in the DRM reaction [16], it has been demonstrated that several support's features, such as the surface basicity, oxygen mobility and storage capacity, as well as the ability of interacting with active phases, influence catalytic performance [64,90].

The support's surface acidic-basic equilibrium may influence the reaction performance in several different aspects. While acidic sites favor CH_4 cracking, which leads to carbon formation [96], the increase in the support's basicity is related to an enhanced removal of carbon deposits, which may lead to higher catalyst stability [97]. Gao et al. [98] indicate that such acidic-basic equilibrium on the catalyst support may also influence the electronic environment of the active sites and further favor/inhibit side reactions such as CH_4 cracking and CO disproportionation.

The addition of MgO to Al_2O_3 support is a well-described method of increasing support basicity for DRM. Song et al. [99] have described the role of MgO as two-fold. First, the basic properties of MgO increase the adsorption of CO_2, which leads to a higher release of oxygen on the support's surface and, in turn, increases the coke resistance via the gasification of carbon deposits (reverse Boudouard reaction). Second, the presence of MgO leads to the formation of a layered double hydroxide, in which the Mg^{2+} and Al^{3+} ions are uniformly dispersed and help decrease the agglomeration of active metal particles and, in turn, increase sintering resistance. On the other hand, excessive basicity may also lead to carbon deposition, decrease metal dispersion, lead to lower H_2/CO ratios and

compromise the overall catalyst performance [98,100]. Bagabas et al. [97] investigated the optimization of the MgO content on Al2O3-supported Ni catalysts for DRM and reported that the highest $H_2/CO = 0.95$ (T = 800 °C, X_{CH_4} = 86%, X_{CO_2} = 91%) was obtained with 2.0 wt% MgO, while higher contents were actually detrimental for the process.

Al-Fatesh et al. [101] evaluated hydrogen production over a series of transition metal-modified (Ti, Mo, Si, W) alumina supports with Ni active phase and reported that adding Si and W increased catalyst thermal stability and yielded 60% and 70% H_2 production, respectively, at T = 700 °C. In this study, the authors highlighted the importance of metal-support interaction on the catalyst activity and showed that harmful interactions between the active phase and the oxide support may significantly compromise the catalyst performance. The formation of poorly active $NiTiO_3$ and $NiMoO$ species, for example, on Ti- and Mo-modified alumina was responsible for a drop in H_2 yields to 30% and 45%, respectively, at T = 700 °C.

Ceria and ceria-modified supports have been investigated for their oxygen storage abilities due to the capacity of cerium to easily change oxidation states from Ce^{4+} to Ce^{3+}. Studies have shown that high oxygen retention accounts for a higher catalyst reducibility, which may lead to increased activity, as well as higher oxygen mobility and carbon gasification effectiveness [102,103]. The oxygen mobility on the catalyst support bulk structure may influence not only the reaction mechanisms, for example, under DRM conditions, but also the metal-support interaction and the overall catalyst stability [104]. On DRM process, the role of oxygen vacancies on the reaction mechanism is two-fold. First, the oxygen vacancies in the lattice of the support act as activation sites for the CO_2 to promote the cleavage of the C–O bonds, which increases the overall amount of oxygen in the support surface. Second, the presence of oxygen vacancies is responsible for oxygen mobility on the bulk catalyst support, which can react with carbon deposits to produce CO and avoid catalyst deactivation by coke deposition [14].

The effect of CeO_2 modification on catalyst supports was investigated by Faria et al. [105] using a ceria-zirconia mixed oxide promotion on alumina-supported Ni catalysts. The use of ZrO_2 in a solid solution with CeO_2 has been proved to increase and stabilize the oxygen vacancies, and, consequently, the oxygen storage capacity of the mixed oxide, via the atomic mobility inside the lattice to accommodate the two components with different atomic radii [106]. The ceria-zirconia promotion over the alumina support enhanced the oxygen mobility of the catalyst and was found to also increase metal-support interaction, but the probable occurrence of RWGS reaction was responsible for a syngas composition below 1.0 (0.75–0.85) [105].

Overall, catalyst development for hydrogen production via DRM is a major challenge, since the reaction also produces CO in the same amount of H_2 ($H_2/CO = 1$) and since side reactions (Equations (3)–(6)) further decrease the H_2/CO ratio. Low hydrogen production resulting from competing reactions, catalyst deactivation due to carbon build-up and particle agglomeration can be overcome by the incorporation of promoters and advances on catalyst synthesis methods. However, there is a lack of literature data on the development of catalysts with high H_2 selectivity in DRM, even in papers dedicated to H_2 via DRM. Further mechanism and kinetic studies are required to better understand how to increase the H_2/CO in this process while maintaining the catalytic performance of the catalysts.

Furthermore, different operating strategies, such as combining DRM with other reforming technologies, can also be used to increase the H_2/CO ratio of the syngas produced. The catalytic aspects of different reforming processes and their combinations are discussed in the next sessions.

3. Alternative Processes for Increased H₂/CO Ratio

CH_4 is a major chemical feedstock and the global primary source for hydrogen, accounting for more than 90% of the annual hydrogen production, via different catalytic reforming processes [107]. While SRM is the most mature and most used technology, several other processes, such as DRM, chemical looping methane dry reforming (CL-DRM),

methane partial oxidation (POM), combined steam and dry-reforming (CSDRM), for example, have been investigated with a focus on reducing the costs and overcoming the environmental and technical challenges of SRM [12]. The H_2-production potential of each of those technologies can be evaluated by their resulting H_2/CO ratio of produced syngas, which is a function of different catalytic and reaction conditions. Different processes can produce syngas with different H_2/CO ratios [108] and, in the case of DRM, this ratio is close to the unity [109], which is suitable for hydrocarbons and methanol production [110,111]. When it comes to hydrogen production, the importance of securing a H_2/CO ratio as close as possible to the unity is even greater [112], for obvious reasons, but when it comes to syngas production, this is also essential for the direct utilization of the syngas with no need for further hydrogen addition.

3.1. Steam Reforming of Methane (SRM)

Steam reforming of methane (SRM) is the most mature and currently applied technology for hydrogen production. This highly endothermic process (Equation (1)) is operated at high temperature (700–1000 °C) at around 3–40 bar to produce a hydrogen-rich syngas with H_2/CO = 3.0 [113]. Figure 2 presents the thermodynamic equilibrium of the SRM process when operated at two different H_2O/CH_4 ratios. When an equimolar H_2O/CH_4 is considered (Figure 2A), H_2 is produced above 180 °C, and this production increases with the temperature increase. Solid carbon is usually obtained in the range between 450 and 800 °C, which can compromise the operation and lead to catalyst deactivation. For H_2O/CH_4 = 3.0 (Figure 2B), the carbon deposits are potentially eliminated and CH_4 can be completely consumed above 700 °C, which justifies the usual operation with excess steam. For hydrogen production purposes, the SRM is usually combined with water-gas shift reaction (WGS; Equation (7)) operated simultaneously to reduce the CO content and boost the hydrogen concentration [114].
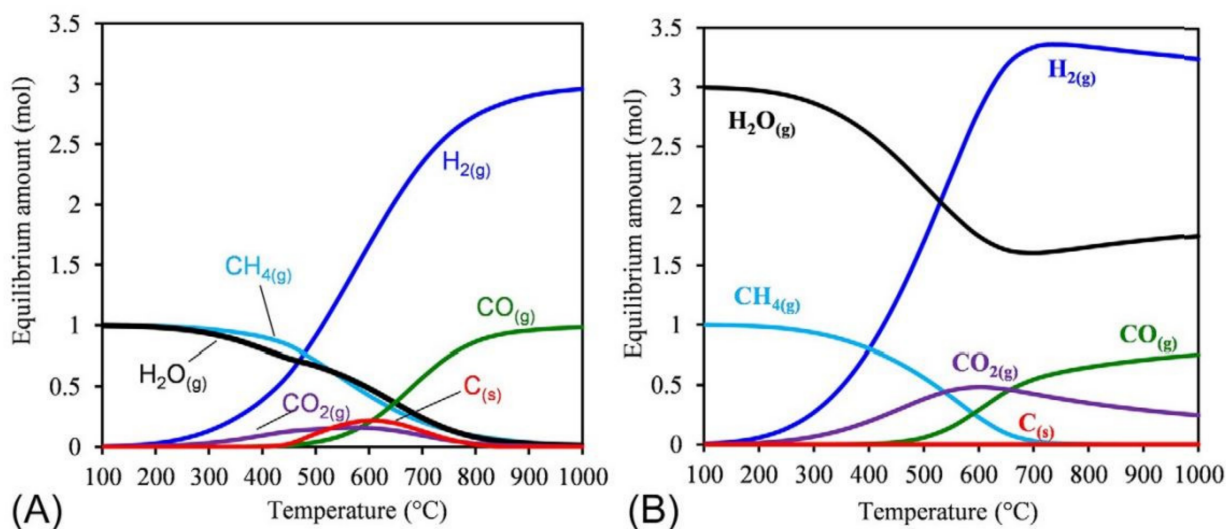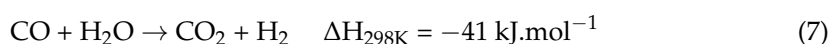

Figure 2. Thermodynamic equilibrium plot for SRM as a function of temperature (T = 100–1000 °C) at 1 bar with (**A**) H_2O/CH_4 = 1.0 and (**B**) H_2O/CH_4 = 3.0. Reprinted with permission from [115]. Copyright 2018 Elsevier.

Alumina-supported Ni-based catalysts are also commonly used in SRM. For this reaction, similar problems with coke deposition and catalyst sintering are also observed, with the aggravating factor that the carbon deposits can not only reduce the catalytic performance but contribute to an increased pressure drop on the reforming reactors. The operation of SRM under excess steam conditions ($H_2O:CH_4$ = 3–5) has been known to help in controlling the carbon deposition over the catalysts [116].

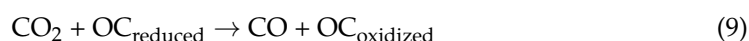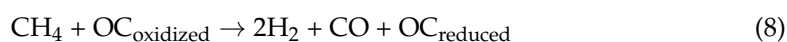$$CO + H_2O \rightarrow CO_2 + H_2 \quad \Delta H_{298K} = -41 \text{ kJ.mol}^{-1} \tag{7}$$

Noh et al. [117] evaluated the performance of Ni-based catalysts supported over calcium aluminate modified SiC for SRM. In this study, the authors aimed to stabilize the H_2 production via SRM by taking advantage of the Lewis basicity of calcium aluminate support to avoid coke deposition. Results revealed that the structured catalysts produced delivered a CH_4 conversion above 80% during 20 h long tests, with H_2 yields above 95% and negligible carbon deposition (T = 850 °C, H_2O:CH_4 = 3). Controlling the coke deposition as a means of enhancing hydrogen production was also the goal of Cho et al. [118] when investigating eggshell-type Ni/$MgAl_2O_4$ pellets as a catalyst for SRM. The authors showed that homo-type catalyst pellets were more prone to carbon deposition and particle agglomeration due to low metal dispersion. On the other hand, superior metal distribution on eggshell-type catalysts led to lower carbon accumulation (2.5% and 39.5%, for eggshell- and homo-type catalyst pellets, respectively) and more stable SRM operation. In this case, CH_4 conversion remained around 50% for TOS = 6 h with high H_2 selectivity (>85%) and overall H_2/CO = 0.80–0.85.

Membrane-type reactors and catalysts have recently been investigated for SRM applications towards hydrogen production. In membrane-based configurations, the produced hydrogen can be removed from the reformed gas while the reaction is still taking place. This sort of purification process can produce a high purity H_2 stream without the requirements of a second downstream stage and alter the reaction equilibrium to promote higher CH_4 conversions. Kim et al. [119] investigated the use of a Pd composite membrane reactor packed with Ru/Al_2O_3 catalyst for CH_4 reforming at mild conditions (T = 500 °C, H_2O:CH_4 = 3). Despite the low operating temperature, CH_4 conversion reached 79.5% when high transmembrane pressure difference (5 bar) was applied to the system. Moreover, the purity of the H_2 permeate stream remained above 97% on 145 h long tests and accounted for 99% hydrogen recovery. Wang et al. [120] reported using Ni-based hollow fiber membrane catalysts for SRM and reaching 99% CH_4 conversion at 800 °C with hydrogen purity above 95%. In both cases, the authors stated that the transmembrane pressure difference proved to be a very important parameter influencing CH_4 conversion for promoting solution and diffusion mechanisms of H_2 through the membrane structure.

3.2. Chemical Looping Dry Reforming of Methane (CL-DRM)

Chemical looping (CL) is a relatively recent process that has been investigated mainly for CO_2 capture and utilization (CCU) [121,122]. In the CL process, a reaction is "broken down" to a series of multiple sub-reactions that take place separately. In this process, materials with a high oxygen storage capacity, here called oxygen carriers (OCs), are used as reaction intermediates that can be recycled along the process and regenerated by oxygen and energy transfer [123,124]. Several CH_4 processing strategies such as partial oxidation and dry reforming can benefit from the stepwise CL strategy. For DRM, chemical looping dry reforming of methane (CL-DRM; Figure 3) consists of two steps (Equations (8) and (9)). First, CH_4 is reacted with an OC and is oxidized to produce a hydrogen-rich syngas mixture (H_2/CO = 2.0). This step is usually called the "reduction step" since the OCs are reduced in the process of syngas production. Second, carbon dioxide is used as an oxidant to recycle the OCs in the usually called "oxidant step", producing CO in the process, which can be recovered separately or mixed with the syngas from the first step [125].
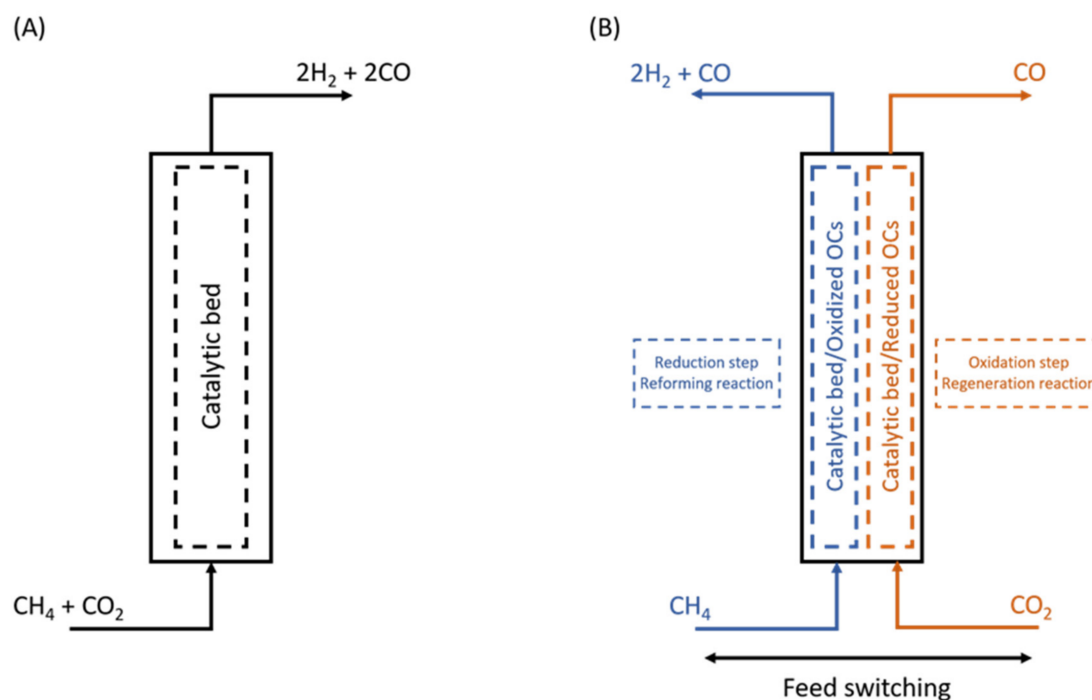
$$CH_4 + OC_{oxidized} \rightarrow 2H_2 + CO + OC_{reduced} \tag{8}$$

$$CO_2 + OC_{reduced} \rightarrow CO + OC_{oxidized} \tag{9}$$

Figure 3. Schematic representation of classic co-fed DRM operation (**A**) and stepwise chemical looping DRM (**B**).

The CL-DRM operation offers numerous advantages when compared to the classical co-feed strategy. Overall, the global process corresponds to a classically operated DRM reaction and still presents an endothermic character. However, the equilibrium of the reaction is no longer dependent solely on the thermodynamics and the reactivity of the reactants and the catalysts, but rather on the redox properties of the OCs, which are the major focus of research and optimization [126]. Chein and Hsu [126] evaluated the thermodynamic equilibrium of CL-DRM as a function of the OC:CH_4 ratio, using Fe_2O_3 as OC. For OC:CH_4 < 1.0, POM is the main observed reaction (Equation (10)), yielding H_2 and CO as the main products (H_2/CO ≈ 2.0). For OC:CH_4 > 1.0, H_2 and CO production decrease as temperature increases, and CH_4 combustion is favored (yielding CO_2 and H_2O) as the OC:CH_4 also increases, reaching total methane combustion for OC:CH_4 > 12.0. Overall, the authors evaluate that an optimal OC:CH_4 = 1.0 could be used to obtain syngas with H_2/CO = 1–2.5 according to the CH_4/CO_2 feed ratio.

Furthermore, two problems observed on DRM can be avoided by the stepwise operation of CL-DRM. The accumulation of carbon on the catalysts (which is now an OC) due to CH_4 dissociation on the reduction step is overcome by the re-oxidation cycle. In this scenario, the deposited coke is converted to CO during the oxidation step. Moreover, since the two reactants, CH_4 and CO_2, are not in contact with CL-DRM operation, the produced H_2 on the reduction step is never in contact with the CO_2 injected on the oxidation step. Hence, the occurrence of RWGS reaction (Equation (6)), which decreases the H_2 selectivity, is also avoided [127,128].

Guerrero-Caballero et al. [129] investigated the performance of a series of CeO_2-based oxygen carriers with Ni, Co and Fe for CL-DRM application. The authors evaluated the influence of preparation method and metal active phase on the catalytic activity of the obtained powders. The catalytic activity of all samples was tested over 12 cycles of CL and presented a relatively stable conversion of both CH_4 and CO_2 over the reduction/oxidation cycles. Ni/CeO_2 presented the best catalytic performance (T = 800 °C, X_{CH_4} = 90%, X_{CO_2} = 85%) and maintained a H_2/CO ratio slightly above 2.0, which is the ratio expected for CL-DRM (Equations (8) and (9)). Despite a lower reactant conversion observed for $CeNi_{0.3}O_y$ (T = 800 °C, X_{CH_4} = 62%, X_{CO_2} = 62%), the catalysts prepared by

co-precipitation presented no coke formation, a steady $H_2/CO = 2.0$ over the 12 CL cycles and no particle sintering, which was related to a better dispersion of the Ni particles on the CeO_2 structure. The influence of the active metal (Ni, Co and Fe) was investigated over wet impregnation-prepared catalysts. The CL-DRM experiments showed that Co/CeO_2 (T = 800 °C, X_{CH_4} = 80%, X_{CO_2} = 85%) catalysts presented a slightly lower CH_4 conversion when compared to Ni/CeO_2, while maintaining a similar H_2/CO between 2.0 and 2.1. Moreover, similar results were obtained at long-term stability tests that comprised 60 CL cycles, with stable H_2/CO ratio between 2.0 and 2.1. As for the Fe/CeO_2 catalyst, very low CH_4 conversion of less than 5% and rapid complete deactivation (after 6 CL cycles) were obtained. These results were related to the formation of poorly active $CeFeO_3$ mixed oxide. Interestingly, the analysis of spent catalysts showed that Ni and Co were not able to follow the oxidation/reduction cycles, i.e., once they were reduced on CL-DRM conditions, the metallic species were not oxidized again, which highlighted the importance of the oxygen storage capacity of CeO_2 on the operation of CL-DRM.

Kim et al. [130] described an efficient CL-DRM process using Ni-Fe-Al mixed oxides as oxygen carriers. In this study, the group showed the superior activity of the trimetallic mixed oxide over binary metallic mixtures, which were submitted to significant deactivation over 12 CL cycles, either by activity loss towards CH_4 decomposition or inefficient coke removal on the oxidation step. Overall, Ni-Fe-Al mixed oxides were able to maintain the catalysts' activity over 20 CL cycles, with no signs of deactivation, to avoid particle agglomeration and activity suppression and to deliver a stable H_2/CO of 2.1. Interestingly, the authors also demonstrated the potential of Ni-Fe-Al mixed oxide for classical co-fed DRM. In this case, results showed that a H_2/CO ratio slightly below 1.0 was achieved for $CH_4:CO_2$ = 1:1 feed at T = 650 °C, with over 80% conversion of both reactants.

Sastre et al. [131] evaluated the perovskite-type $La_{0.9}Sr_{0.1}FeO_3$ supported on yttria-stabilized-zirconia (YSZ) for DRM and CL-DRM and reported a high H_2 production ($H_2/CO = 6.5$) during the reforming step for the looping operation. The authors evaluated the DRM process at 850 °C for 24 h and obtained an H_2/CO between 0.95 and 0.98 during the tests. For the CL operation, 20 min looping cycles were performed up to 7 h. The authors reported that for the reforming step (CH_4 injection), a predominant CH_4 cracking (Equation (3)) reaction took place and yielded high H_2/CO ratios (up to 6.5) with high coke formation. On the other hand, coke was successfully removed during the oxidation step (CO_2 injection) and the catalysts did not present significant deactivation during CL operation.

3.3. Combined Steam and Dry Reforming of Methane (CSDRM)

A combination of steam and dry reforming of methane (CSDRM) has been investigated as an alternative for modulating the H_2/CO ratio with a focus on increasing H_2 production and allowing for a higher versatility on the chemical and fuels production steps [132]. The use of steam on the feed for DRM may account for a reduced coke formation by oxidation of adsorbed CH_X that could otherwise lead to carbon deposits [133]. In addition, studies have shown that the convenient adjustment of the CH_4/H_2O ratio on feed composition leads to the desired modulation of H_2/CO ratio [132,134].

Figure 4 presents the thermodynamic equilibrium of CSDRM at different pressures, considering a $CH_4:CO_2:H_2O$ feed ratio of 3:1:2. As both SRM and DRM have an endothermic aspect, the conversion of all reagents is favored at higher temperatures. Lower pressures are related to a decrease in both CH_4 and CO_2 conversion and lower H_2 selectivity. H_2/CO ratio decreases with the temperature increase and stabilizes around 2.0 in the range of 800–1000 °C [135].
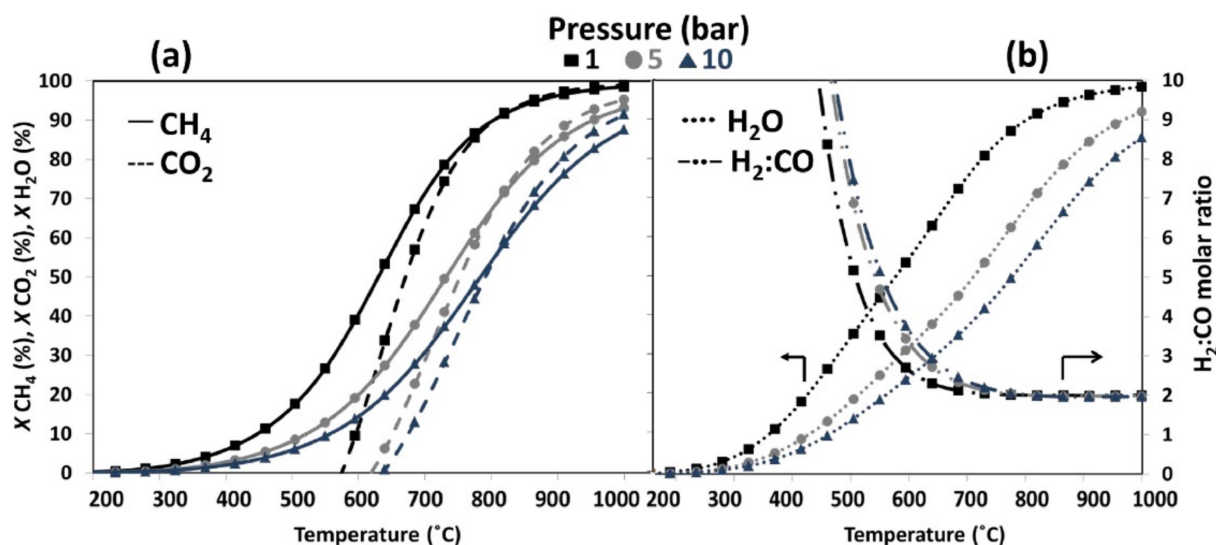
Figure 4. Thermodynamic equilibrium plot for POM as a function of temperature (T = 200–1000 °C) at 1–10 bar with CH_4:CO_2:H_2O = 3:1:2. (**a**) CH_4 and CO_2 conversion levels; (**b**) H_2O conversion and H_2/CO ratio profile. Reprinted with permission from [135]. Copyright 2020 Elsevier.

Dan et al. [136] investigated the performance of 10 wt% Ni/Al_2O_3 catalyst, which is a classical reforming catalyst, on CSDRM conditions. The study has shown that a higher hydrogen production can be achieved by the CSDRM operation at 700 °C with 100% conversion of CH_4 and a high H_2O/CO_2 ratio on the inlet feed. For H_2O/CO_2 ratios of 2.5, 7.3 and 12.7, the H_2/CO ratios achieved on this study were 2.2, 5.0 and 8.0, respectively. In addition, the stability of the 10 wt% Ni/Al_2O_3 catalyst was evaluated for 24 h at CSDRM conditions and 100% CH_4 conversion was maintained for the whole test when H_2O/CO_2 = 7.3 and 12.7 were used at 700 °C. Moreover, analysis of spent catalyst showed no oxidation or size changes of Ni sites, indicating that deactivation by catalyst sintering or oxidation was not triggered on the reaction conditions, and no carbon deposits were detected.

Batebi et al. [137] reported the influence of feed composition on the CSDRM activity and final hydrogen yields over Ni- and Pd-based catalysts supported on Al_2O_3. Mono- and bimetallic catalysts were prepared by sol-gel method and tested for CSDRM at 500–1000 °C with various (CO_2 + H_2O)/CH_4 ratios (1–3) and CO_2/H_2O ratios (1–3) under atmospheric pressure. A central composite experimental design was used to evaluate the statistical significance of the influence of each reaction condition on the final CH_4 conversion and H_2 yield. Based on the ANOVA results, the authors showed that higher temperatures (T > 700 °C) were crucial to achieve higher CH_4 conversions (>75%) due to the endothermic character of both SRM and DRM reactions. As for the influence of feed composition, the authors confirmed that the CO_2/H_2O ratio had no significant impact on the final CH_4 conversion and H_2 yields. However, when the amount of CO_2 was higher in the inlet feed, lower H_2/CO ratios were obtained. Finally, higher H_2 yields were favored by lower (CO_2 + H_2O)/CH_4 ratios at temperatures lower than 1000 °C, when competitive RWGS reaction takes place and reduces the H_2 final production.

3.4. Partial Oxidation of Methane (POM)

The catalytic partial oxidation of methane (POM) has attracted attention for being a more energy-efficient process when compared to commercial SRM. The fast kinetics of POM lead to a good response time and system compactness, while its exothermic character is less energy demanding and avoids the requirements of high temperature steam [138]. In the partial oxidation process, CH_4 (or other hydrocarbons) is reacted with stoichiometric amounts of pure oxygen and yields a H_2/CO ratio of 2.0 for the produced syngas (Equation (10)), which is suitable for Fischer-Tropsch synthesis [139]. However, controlling the

reaction selectivity to avoid total combustion can be challenging [140]. Figure 5 presents the thermodynamic equilibrium for POM as a function of temperature for different operating pressures for a stoichiometric feed ($CH_4:O_2$ = 2.0, Equation (10)). Enger et al. [141] highlight that, at higher pressures, higher temperatures are required for obtaining a high selectivity towards H_2 and CO (Figure 5b,c). In addition, the authors also comment that high H_2 selectivity (>80%) can be obtained for temperatures as low as 550 °C if $CH_4:O_2$ ranges between 2.0 and 5.0.

Figure 5. Thermodynamic equilibrium plot for CSDRM as a function of temperature (T = 700–1200 K) at 1–20 bar with $CH_4:O_2$ = 2.0. (**a**) CH_4 conversion; (**b**) H_2 selectivity; (**c**) CO selectivity. Reprinted with permission from [141]. Copyright 2008 Elsevier.

Classical noble- and transition-metal-based catalysts are the most reported for POM, and carbon deposition is also a major trigger for catalyst deactivation. Moreover, the temperature gradients resulting from the exothermic POM reaction increase the probability of catalyst deactivation due to particle sintering, which leads to more challenges on catalyst development [139].

$$CH_4 + \frac{1}{2}O_2 \rightarrow 2H_2 + CO \qquad \Delta H_{298K} = -36 \text{ kJ.mol}^{-1} \qquad (10)$$

Alvarez-Galvan et al. [139] evaluated the performance of different Ni-based catalysts for hydrogen production via POM. Catalysts containing 5 wt% of Ni doped on Al_2O_3, CeO_2, La_2O_3, MgO and ZrO_2 supports were tested for POM activity under stoichiometric feed conditions at T = 750 °C and atmospheric pressure. Among the prepared catalysts, 5 wt% Ni/MgO and 5 wt% Ni/La_2O_3 presented low activity and rapid deactivation, due to the formation of non-catalytic phases between the metal and the oxide support. The alumina-supported 5 wt% Ni/Al_2O_3 revealed to be the most efficient and most stable catalytic system, with >80% CH_4 conversion and H_2 yields throughout the catalytic tests. In addition, the authors showed that Rh-promotion over the Ni/Al_2O_3 catalyst was responsible for a slight increase in CH_4 conversion and H_2 yield up to 90%. Finally, the H_2/CO ratio for the obtained syngas was stable around 2.5 for the Ni/Al_2O_3 catalyst with or without Rh-promotion. Ding et al. [142] also investigated the hydrogen production via POM over Ni-based catalysts and reported the use of mesoporous oxides La_2O_3, Yb_2O_3, ZrO_2 and CeO_2 for the modification of SiO_2 support. The catalysts were prepared with a 10 wt% Ni loading and tested for their POM activity under stoichiometric feed conditions, atmospheric pressure and T = 800 °C. The authors demonstrated that the modifications with mesoporous solid oxides were able to increase Ni dispersion on the support, which increases catalytic activity and CH_4 conversion > 75% (reaching 90% for 10 wt% Ni/ZrO_2-SiO_2). Moreover, the authors reported that hydrogen production via POM can profit from oxygen mobility of oxide supports such as ZrO_2, which promotes the combustion-reforming mechanism. In this mechanism, CH_4 and O_2 first react to form CO_2 and H_2O, followed by a combined steam and dry reforming promoted by the combustion products and the excess CH_4 [139]. In this case, H_2 selectivity increased almost 20% and the final H_2/CO ratio of produced syngas stabilized at 3.0.

3.5. Methane Tri-Reforming (TRM)

The methane tri-reforming (TRM) process refers to a combination of the SRM, DRM and POM processes, in which methane is reacted with a mixture of steam, CO_2 and oxygen to produce syngas [143]. According to its thermodynamic aspects (Figure 6), TRM is favored at higher temperatures ($T \geq 700\ °C$) due to the already discussed endothermic aspects of the individual reforming reactions (SRM and DRM) and the stability of the reactants. Moreover, lower pressures (1 bar) also favor the TRM equilibrium, although typical reforming reactors usually operate at higher pressures (3–30 bar) to decrease reactor size and meet high-pressure requirements for syngas downstream processes [115,144]. Under stoichiometric conditions (2 mol of CH_4, 1 mol of H_2O, 1 mol of CO_2, 0.1 mol of O_2), CH_4 is almost completely converted (>98%) above 850 °C, oxygen is completely consumed via POM and high syngas selectivity of 1.65 is reached above 800 °C [115]. However, the main advantage of the TRM process is the adjustable H_2/CO ratio of the produced syngas according to the feed composition, which makes TRM a versatile CH_4 reforming process that can be controlled for various downstream applications, such as methanol or Fischer-Tropsch synthesis [145].
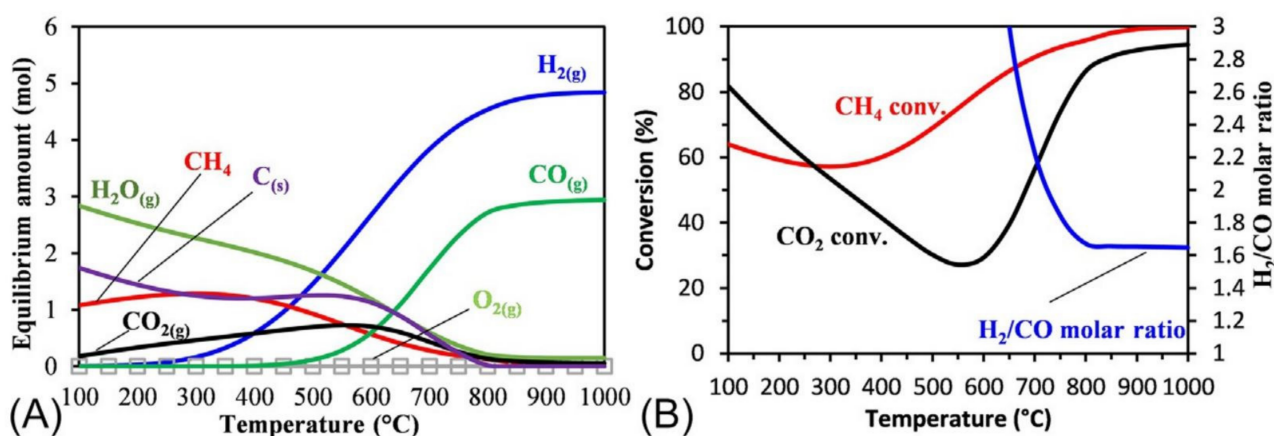

Figure 6. Thermodynamic equilibrium plot for TRM as a function of temperature (T = 100–1000 °C) at 1 bar with $CH_4:CO_2:H_2O:O_2$ = 2:1:1:0.1. (**A**) Equilibrium amounts for all species; (**B**) CH_4 and CO_2 conversions, H_2/CO ratio profile. Reprinted with permission from [115]. Copyright 2018 Elsevier.

As a combination of different catalytic reforming processes, TRM also profits from the low cost and known catalytic activity of Ni-based catalysts for reaction with C–H bonds. Maciel et al. [146] evaluated the performance of 5.75 wt% Ni/Al_2O_3 catalyst for TRM under 1 bar and feed composition $CH_4:CO_2:H_2O:O_2$ = 1.0:0.49:0.3:0.04. The authors reported that the highest hydrogen yield of 37% was achieved at temperatures higher than 850 °C. The competing RWGS reaction was predominant for T < 850 °C and decreased the H_2 yield to 4.4%. Majewski and Wood [147] prepared core-shell-type 11 wt% Ni/SiO_2 catalysts for TRM and reported high hydrogen production and low coke deposition for T = 750 °C. At this temperature, SRM and DRM reactions were favored, which increased H_2 production, while for $T \geq 800\ °C$, RWGS took place and decreased the overall H_2/CO ratio to 1.5–1.7. In this study, the authors reached a H_2/CO ratio of 2.6 with 73% and 56% of CH_4 and CO_2 conversion, respectively, and low carbon formation (5.0 mg g^{-1} catalyst) for a feed composition of $CH_4:CO_2:H_2O:O_2:He$ = 1.0:0.5:0.5:0.1:0.4.

Pino et al. [148] investigated hydrogen production by TRM over 1.76 wt% Ni/CeO_2 catalyst at T = 800 °C and described the impact of La-doping and different feed compositions on the final H_2/CO ratio. The authors reported that La modifications on the catalysts were able to increase the presence of oxygen vacancies on the ceria support and enhanced Ni dispersion, which account for high CH_4 (96%) and CO_2 (86%) conversions. However, the La-doping did not show any significant impact on hydrogen production. The modifications on feed composition, on the other hand, were able to modulate the final H_2/CO ratio of the

syngas. The authors demonstrated that the H_2/CO ratio could drop from 2.8 to 1.3 when the inlet molar ratio of CO_2/H_2O varied from 0.0 (in the absence of CO_2) to 2.6. According to Pham Minh et al. [145], the modulation on the H_2/CO ratio as a function of the feed composition is due to competitive CH_4 reforming reactions that take place as a result of the presence of multiple oxidants (CO_2, H_2O and O_2) on the TRM process.

García-Vargas et al. [149] investigated the influence of different support materials for 5 wt% Ni-based catalysts. The authors synthesized four different catalysts supported over Al_2O_3, yttria-stabilized-zirconia (YSZ), CeO_2 and silicon carbide (β-SiC). The high thermal conductivity, mechanical strength and chemical inertness of β-SiC proved to be excellent catalytic features for TRM. The 5 wt% Ni/β-SiC presented the highest H_2/CO ratio of 2.0 on the catalytic tests. Moreover, both 5 wt% Ni/β-SiC and 5 wt% Ni/CeO_2 catalysts showed high CH_4 conversion and the highest reaction rates (11.70×10^4 mol s^{-1} g$_{Ni}$$^{-1}$ and 11.13×10^4 mol s^{-1} g$_{Ni}$$^{-1}$, for 5 wt% Ni/$CeO_2$ and 5 wt% Ni/β-SiC, respectively).

4. Large-Scale Applications of DRM

The potential benefits of industrial implementation of DRM have driven several research groups into investigating not only the catalyst optimization aspects but also the process scaling up to commercial level [150]. Over the years, different groups have evaluated several aspects of the DRM process on a semi-pilot and pilot scale, aiming at bringing it into commercial application. Kahle et al. [151] have demonstrated the use of Pt-based catalysts for DRM at 850–950 °C and 20 bar and have considered different process aspects such as catalyst position, temperature gradient and feed composition aiming at reducing coking formation at pilot-scale conditions. The authors reported reaching a $H_2/CO = 0.78$ at T = 850 °C, 20 bar, $CH_4:CO_2 = 1:1$. In addition, studies have also addressed other aspects, such as the type of reactor [152] and catalyst structure (in the case of different shapes of pelletized catalysts) [150], aiming at maximizing DRM activity and reducing deactivation rates at pilot scale.

While CH_4 reforming technologies, such as autothermal reforming and steam reforming, are already used in industrial scale, the commercial application of DRM has been limited as a part of some industrial processes, such as the CALCOR™, SPARG™ and MIDREX™ processes [153]. Although such processes do not target H_2 production, understanding the commercial-level applications of DRM is a valuable way of assessing the advantages and limitations of the technology. Table 2 presents a summary of the main aspects of the pilot- and commercial-scale applications of DRM.

Table 2. Summary of large-scale DRM applications.

Technology	Catalyst	Feed Composition	Operation Conditions	H₂/CO Ratio	TRL	Process Application	Ref.
DRM	10 wt% Ni/Al₂O₃-MgO	CO₂:CH₄:N₂ = 2:1:0.5	600 °C, 1 bar	>1.0	Semi-pilot scale	Syngas production	[150]
DRM	Pt-based	CH₄:CO₂:Ar = 1:1:0.05	850–950 °C, 20 bar	0.7–0.8	Pilot-scale	Syngas production	[151]
CALCOR™ (Caloric GmbH)	Ni-based	CH₄, LPG, CO₂. Feed composition not reported.	Low pressure, high temperature	0.42–1.0	Commercial	CO production	[154,155]
SPARG™ (Haldor-Topsoe)	Partially sulfur-poisoned Ni	CH₄, H₂O, CO₂, H₂S (pre-reforming, for catalyst passivation). CO₂/CH₄ = 0.07–2.5; H₂O/CH₄: 0.1–0.26	875–945 °C	0.55–3.2	Commercial	Syngas production	[156–158]
MIDREX™ (Midrex Technologies)	Ni-based, supported on α-Al₂O₃ and/or MgO	CH₄:CO₂:H₂O = 1:1:1	850–1000 °C, 2–3 bar	1.7–2.5	Commercial	Metallic Fe production	[159–161]
DRYREF™ (Linde and BASF)	Ni-based oxide-supported tablets (4-hole quadrilobes)	CH₄, H₂O, CO₂ (S/C < 1.8)	800–950 °C, 20–40 bar	1.0–3.0	Commercial demonstration (since 2019)	CO and H₂ production	[162,163]

TRL—Technology readiness level; LPG—Liquified petroleum gas.

The CALCOR™ process (Caloric GmbH) aims at the production of highly CO-concentrated syngas (Figure 7). In the first stage of this process, syngas with a low H_2/CO ratio (0.42) is

produced from the dry reforming of liquefied petroleum gas (LPG) or natural gas (NG) with excess CO_2, over a Ni-based catalyst [164]. In this process, the coke deposition is minimized by using a catalyst bed with different stages of catalyst reactivity and different catalyst geometries [165]. As DRM is a highly endothermic process [166], part of the fuel is burnt to provide heat for the reaction. The process outlet stream is a mixture of CO, CO_2, H_2, H_2O and traces of unreacted CH_4. The stream is cooled for H_2O removal, then it is scrubbed through packed towers with monoethanolamine (MEA) or methyldiethanolamine (MDEA) for CO_2 removal and, finally, is purified by a pressure swing adsorption unit (PSA) for H_2 separation that would operate according to the CO purification requirements (can reach up to 99.95% CO) [155]. The unreacted CO_2 is recycled to the reformer and the H_2 produced during the reaction is either burnt as fuel or sold as a separate product. Despite the toxicity, CO is an important chemical building block for the production of several carbon-based chemicals such as acetic acid and phosgene [155,164,167].
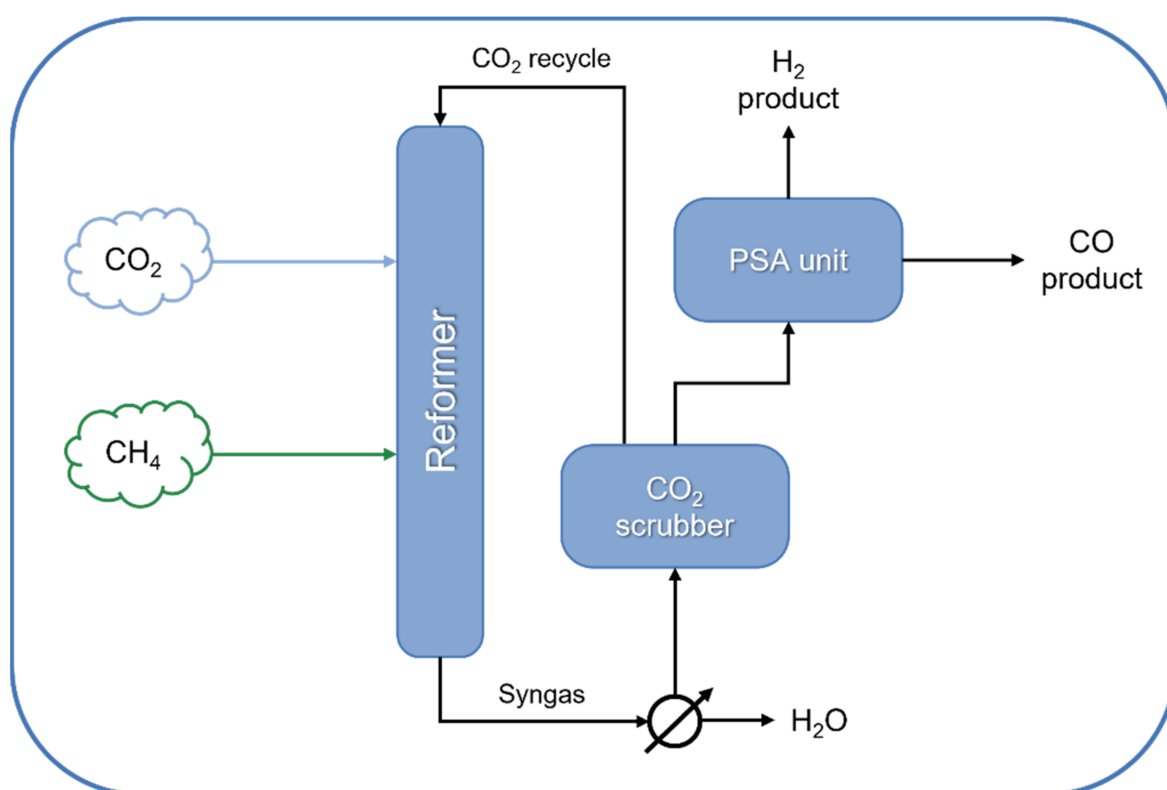

Figure 7. Simplified block diagram of the CALCOR™ process for CO production [155]. PSA—Pressure swing adsorption.

The SPARG™ (sulfur passivated reforming) process, which was initially designed by Haldor-Topsoe and commercialized by Sterling Chemical Inc. in 1987, is another example of an industrial application of DRM for the production of syngas with lower H_2/CO ratios. This process takes advantage of the already existing infrastructure for SRM, combining characteristics of both SRM and DRM, and it is able to deliver syngas with a H_2/CO ratio ranging from 1.8 to 3.0 [158,165,168]. The process can operate with different CO_2 and H_2O mixtures and can be considered a type of CSDRM [165]. In this process (Figure 8), sulfur is selectively used to poison the catalyst sites that are most active for coke formation in order to minimize it during the reaction, while keeping part of the reforming activity [168]. The SPARG™ process is operated between 915 °C and 945 °C, and the coke formation over the Ni catalyst is minimized by the sulfur pretreatment that passivates the main coke-active sites on the catalyst [165].
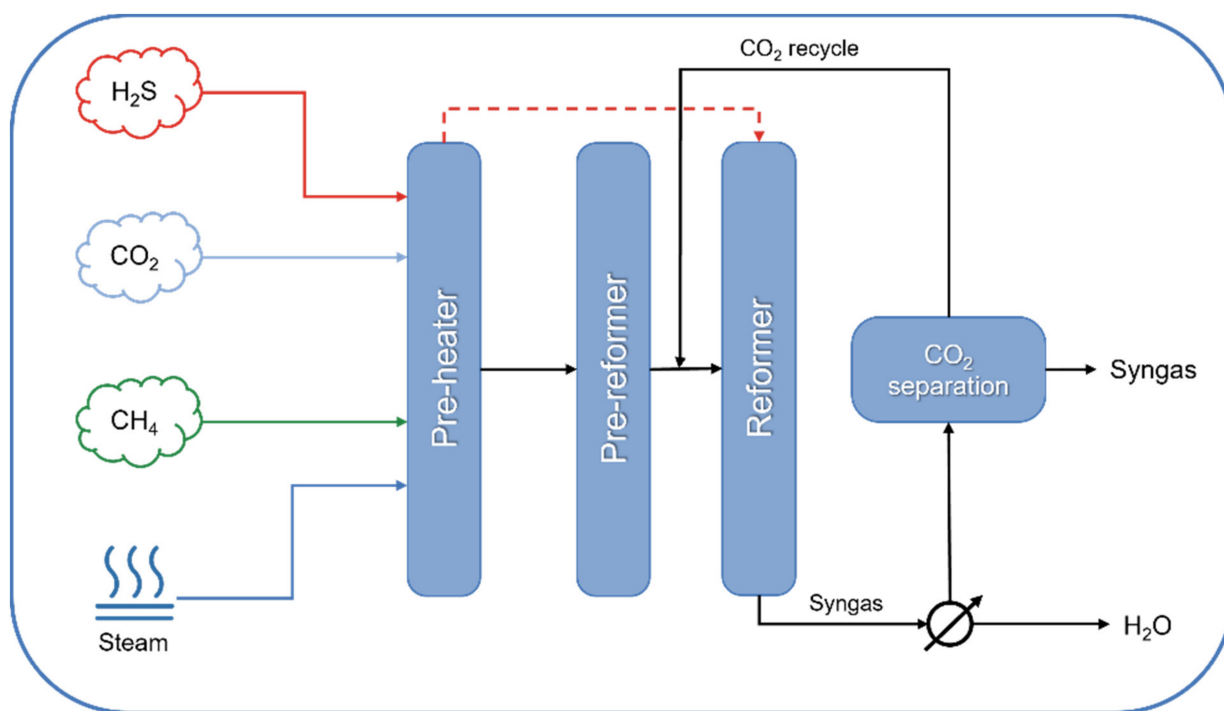
Figure 8. Simplified block diagram of the SPARG™ process for syngas production [106].

Both the CALCOR™ and the SPARG™ processes are designed to prevent the formation of coke under DRM conditions. Unfortunately, these processes require specific conditions for their full applicability. Therefore, in order to reduce these barriers and increase the range of applicability of these processes, a better understanding of the mechanisms of coking and measures related to the development of catalysts are necessary, as well as the choice of the reactor material [158].

The MIDREX™ process (Figure 9) was developed in the 1960s and remains, to this day, a leading process in the field of the direct reduction technology [169]. This process takes advantage of a combined DRM and SRM process to produce syngas which is later used as a reducing agent for the production of metallic iron [161]. In the MIDREX™ process, the reformer is fed with a mixture of CO_2:CH_4:H_2O = 1:1:1. The MIDREX reforming process is performed over a Ni-based catalyst supported on α-alumina, MgO or a combination thereof, and operated between 850 and 1000 °C at 1.9–3.0 bar. Basic promoters such as Zr, Ce and La are also frequently used on commercial catalysts for this process, which can increase the overall basicity of the catalysts, prevent carbon deposition and stabilize Ni particles [160,161]. Although detailed information on the syngas produced via the MIDREX™ process is not available, since the syngas is not actually the final product, modeling has indicated that the H_2/CO ratio of the syngas should be in the range between 2.0 and 2.5 [160]. The MIDREX™ process operates commercially since the 1970s and has currently over 100 plants installed in 21 countries, having decommissioned only the pilot- and demonstration-scale plants built pre-1975 [159].

Linde and BASF have recently collaborated to the advancement of DRM industrial implementation. The DRYREF™ technology (Figure 10) has been developed by Linde with the aims of not only contributing to the efforts towards anthropogenic CO_2 utilization, but also for reducing the capital (CAPEX) and operational (OPEX) costs of CH_4 reforming technologies [170]. The process is based on an innovative catalyst developed by BASF, the SYNSPIRE™ G1-110, which is a Ni-based oxide-supported catalyst, specially designed to prevent coke formation and to operate at pressurized reforming conditions (20–40 bar) [162]. The DRYREF™ technology is an application of CSDRM, in which the use of CO_2 is designed to reduce the energy requirements of the full SRM process, due to the energy-demanding steam production step. In the process developed by Linde, a lower steam-to-carbon ratio

(S/C < 1.8) is combined with CO_2 capture and recycling in order to reduce the overall carbon footprint of the process and the high steam requirements of SRM (S/C $\geq$ 2.5). The result is an overall 5% and 3% reduction in OPEX and CAPEX, respectively, and a variable syngas H_2/CO ratio (dependent on the initial S/C ratio) in the range of 1.0–3.0, which can be suitable for several downstream processes, such as aldehydes, methanol, acetic and formic acid synthesis [163]. The project started in 2010 and is currently on commercial demonstration scale since 2019, after the commissioning of the Linde Pilot Reformer, in Pullach, Germany [170].
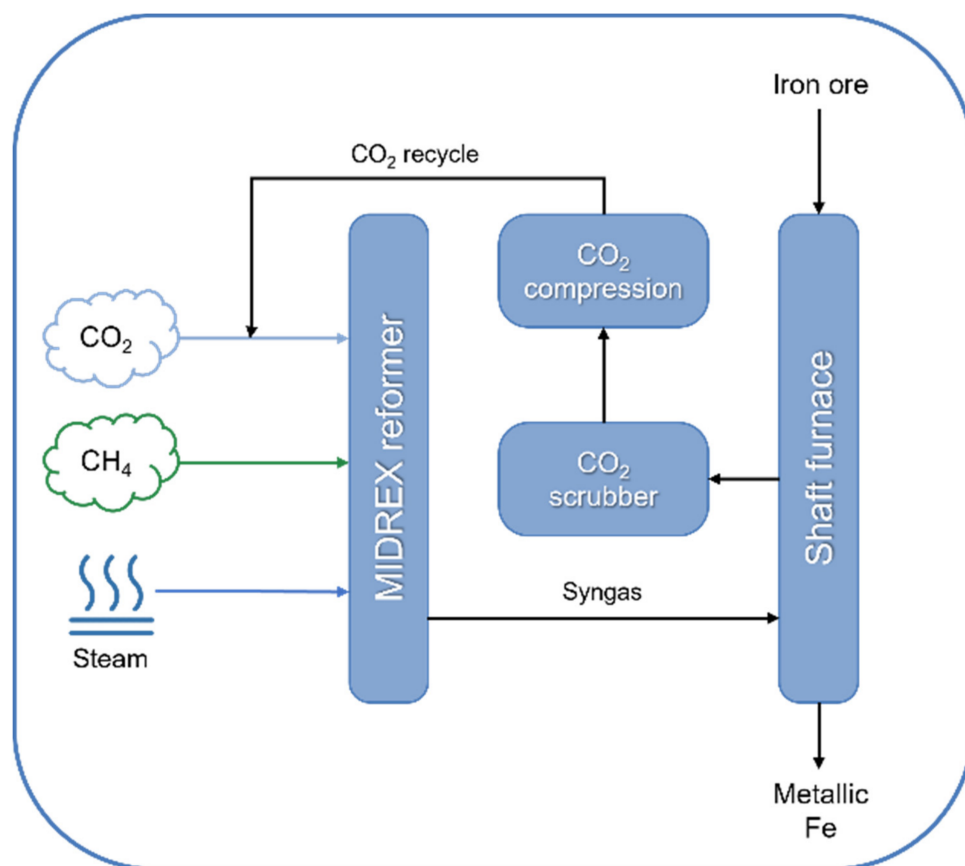

Figure 9. Simplified block diagram of the MIDREX™ process for metallic iron production [159].
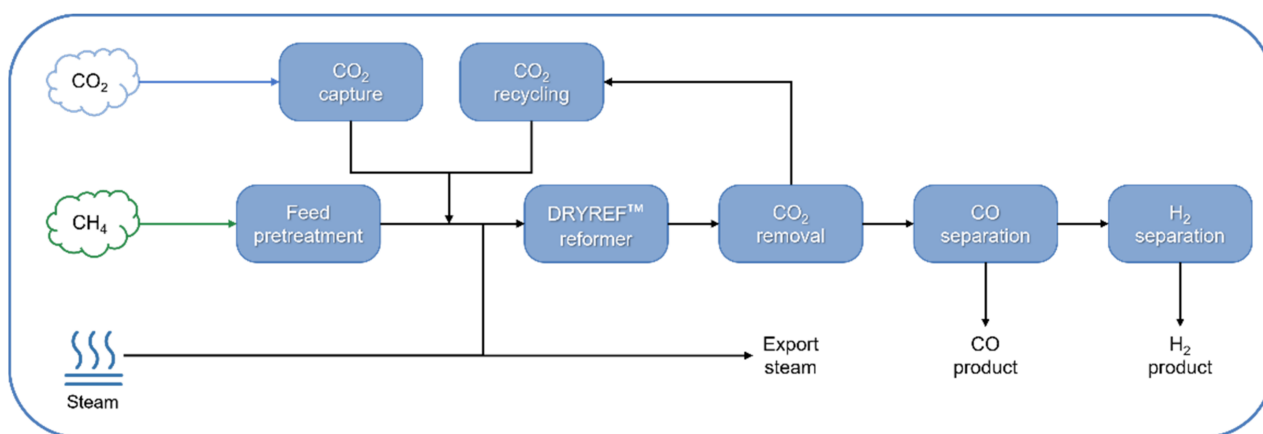

Figure 10. Simplified block diagram of the DRYREF™ process for CO and H_2 production [162].

The highly endothermic aspect of DRM requires high operating temperatures for high syngas yields, which promotes undesired parallel reactions and deactivation of conventional catalysts by sintering mechanisms. In addition, the limited stability of conventional

reactor materials at the required high temperatures further hinders the application of this process in industrial scale. Technological advancements are therefore required to obtain both reactors and catalysts that can withstand reaction temperatures above 1000 °C [171].

None of the processes presented above target the production of H_2 as the final product. Hence, large-scale data on DRM aiming at a high H_2/CO ratio, as well as detailed information on sizing and overall energy efficiency of the process and specific facilities, are not available in the open literature. Besides catalytic development and process optimization at laboratory scale, life-cycle assessment and techno-economic analysis of this process are also required to evaluate the real environmental advantages of producing H_2 through this pathway and to assess its economic viability.

5. Conclusions and Perspectives

DRM has been extensively reported in the recent literature as a possible alternative pathway for sustainable H_2 production since it uses CH_4 and CO_2 (two main GHGs) as feedstock. However, this process still suffers from catalyst deactivation in the harsh reaction conditions, mainly due to coking and sintering of the active phase. Moreover, economic issues must also be taken into account, especially when H_2 production is considered, since this reaction also produces 1 mol of CO per mol of H_2 and side reactions (Equations (3)–(6)) may also occur, further decreasing the H_2/CO ratio of the syngas produced. However, as presented in Section 2, the focus of catalyst development has been on improving the stability and activity of catalysts and the H_2/CO ratio of the syngas produced is often secondary, even in papers that target DRM as a pathway for H_2 production. Some of the works cited in Section 2 suggested that low metal loadings could lead to small metal particles that would be more available to the reactants and could increase the H_2 production. High surface area of catalysts and high reducibility of the active phase would increase its activity and increase H_2 production. Finally, tuning process conditions, such as CH_4/CO_2 feed ratio, can also improve CH_4 decomposition and increase the H_2/CO ratio of the syngas produced. However, there is still a lack of detailed data on the literature dedicated to improving the catalyst design to favor higher H_2/CO ratios via this reaction.

Some of the technical and economic challenges in DRM for H_2 production could be partially overcome by either using a chemical looping process or by combining DRM with other technologies, such as steam reforming and partial oxidation. DRM operated in a chemical looping is an interesting process, since only CH_4 and CO_2 are used as feedstock, but the process produces syngas with H_2/CO generally around 2.0, which is higher than the H_2/CO obtained in classical DRM reactions. This is achieved by using oxidation and reduction cycles so the H_2 produced from CH_4 oxidation with the catalyst is not in contact with the CO_2, which prevents the RWGS reaction and assures a high H_2/CO ratio. However, catalyst development is still required to improve their oxygen storage capacity before utilization at larger scales. Combined steam and dry reforming of methane (CSDRM) have also been considered as an alternative process to the classical DRM to improve the H_2/CO ratio. Steam is added to the feed allowing the production of syngas with a flexible H_2/CO ratio up to 8.0 depending on the amount of steam used. The addition of steam also contributes to preventing carbon depositions and catalyst deactivation. However, issues related to the endothermicity of this reaction must also be considered. Methane tri-reforming, which adds steams and oxygen to the feed mixture, has also been investigated, since it can produce syngas with a higher H_2/CO of around 3.0. This process can also cope for the endothermicity of the reactions, since part of the CH_4 is combusted to generate heat for the reactions. However, there are issues related to catalyst deactivation via sintering and vapor-solid reactions that occur on the surface of catalysts.

Due to these issues related to catalyst performance and thermodynamics, only very few industrial processes use DRM at large scale. However, none of them aim at the production of H_2 or of syngas with a high H_2/CO ratio. The CALCOR™ process produces a CO-rich syngas while the SPARG™ process produces syngas with a H_2/CO ratio lower than 1.

Finally, the MIDREX™ process does not target H$_2$ or syngas as the final product. The syngas produced in this process is used as a reducing agent for metallic iron production.

DRM is definitely a very promising process for the production of energy vectors, especially considering that GHGs are used as feedstock. However, the role that it will play in the future large scale of H$_2$ production is still debatable. DRM still faces technical and economic issues related to catalyst deactivation and the endothermicity of the reaction. Moreover, there are still a lot of data missing on how to improve the performance of the catalysts and of the process to increase the selectivity to H$_2$. Mechanistic and kinetic studies for better understanding the performance of the catalysts for H$_2$ production and optimizing reactor design and process conditions are still required before the use of this process at larger scale. Finally, there is also a lack of data on life-cycle and techno-economic analysis of DRM for H$_2$ production. Estimating the costs and the carbon intensity of H$_2$ produced via this process are crucial to better understand the environmental and economic potential of using DRM for H$_2$ production.

Author Contributions: Conceptualization, F.G.M.d.M. and B.R.d.V.; data curation, F.G.M.d.M. and F.W.B.L.; writing—original draft preparation, F.G.M.d.M., F.W.B.L. and B.R.d.V.; writing—review and editing, B.R.d.V. All authors have read and agreed to the published version of the manuscript.

References

1. International Energy Agency. *The Future of Hydrogen*; IEA: Paris, France, 2019; Available online: https://www.iea.org/reports/the-future-of-hydrogen (accessed on 9 February 2022).
2. Rego de Vasconcelos, B.; Lavoie, J.-M. Recent Advances in Power-to-X Technology for the Production of Fuels and Chemicals. *Front. Chem.* **2019**, *7*, 392. [CrossRef] [PubMed]
3. Chi, J.; Yu, H. Water electrolysis based on renewable energy for hydrogen production. *Chin. J. Catal.* **2018**, *39*, 390–394. [CrossRef]
4. Dincer, I.; Zamfirescu, C. Hydrogen Production by Electrical Energy. In *Sustainable Hydrogen Production*; Elsevier: Cambridge, MA, USA, 2016; pp. 99–161. ISBN 9780128015636.
5. le Saché, E.; Reina, T.R. Analysis of Dry Reforming as direct route for gas phase CO$_2$ conversion. The past, the present and future of catalytic DRM technologies. *Prog. Energy Combust. Sci.* **2022**, *89*, 100970. [CrossRef]
6. Chein, R.Y.; Chen, Y.C.; Yu, C.T.; Chung, J.N. Thermodynamic analysis of dry reforming of CH$_4$ with CO$_2$ at high pressures. *J. Nat. Gas Sci. Eng.* **2015**, *26*, 617–629. [CrossRef]
7. Nishimura, A.; Takada, T.; Ohata, S.; Kolhe, M.L. Biogas Dry Reforming for Hydrogen through Membrane Reactor Utilizing Negative Pressure. *Fuels* **2021**, *2*, 194–209. [CrossRef]
8. Thanh Son, P.; Abdoul Razac, S.; Rêgo de Vasconcelos, B.; Nzihou, A.; Sharrock, P.; Grouset, D.; Doan, P.M. Hydroxyapatite supported bimetallic cobalt and nickel catalysts for syngas production from dry reforming of methane. *Appl. Catal. B Environ.* **2017**, *224*, 310–321. [CrossRef]
9. Rego de Vasconcelos, B.; Pham Minh, D.; Martins, E.; Germeau, A.; Sharrock, P.; Nzihou, A. Highly-efficient hydroxyapatite-supported nickel catalysts for dry reforming of methane. *Int. J. Hydrogen Energy* **2019**, *45*, 18502–18518. [CrossRef]
10. Rego de Vasconcelos, B.; Pham Minh, D.; Lyczko, N.; Phan, T.S.; Sharrock, P.; Nzihou, A. Upgrading greenhouse gases (methane and carbon dioxide) into syngas using nickel-based catalysts. *Fuel* **2018**, *226*, 195–203. [CrossRef]
11. Farooqi, A.S.; Al-Swai, B.M.; Ruslan, F.H.; Mohd Zabidi, N.A.; Saidur, R.; ad Syed Muhammad, S.A.F.; Abdullah, B. Catalytic conversion of greenhouse gases (CO$_2$ and CH$_4$) to syngas over Ni-based catalyst: Effects of Ce-La promoters. *Arab. J. Chem.* **2020**, *13*, 5740–5749. [CrossRef]
12. Chen, L.; Qi, Z.; Zhang, S.; Su, J.; Somorjai, G.A. Catalytic hydrogen production from methane: A review on recent progress and prospect. *Catalysts* **2020**, *10*, 858. [CrossRef]
13. Oyama, S.T.; Hacarlioglu, P.; Gu, Y.; Lee, D. Dry reforming of methane has no future for hydrogen production: Comparison with steam reforming at high pressure in standard and membrane reactors. *Int. J. Hydrogen Energy* **2012**, *37*, 10444–10450. [CrossRef]
14. Pakhare, D.; Spivey, J. A review of dry (CO$_2$) reforming of methane over noble metal catalysts. *Chem. Soc. Rev.* **2014**, *43*, 7813–7837. [CrossRef] [PubMed]
15. Yentekakis, I.V.; Goula, G.; Hatzisymeon, M.; Betsi-Argyropoulou, I.; Botzolaki, G.; Kousi, K.; Kondarides, D.I.; Taylor, M.J.; Parlett, C.M.A.; Osatiashtiani, A.; et al. Effect of support oxygen storage capacity on the catalytic performance of Rh nanoparticles for CO$_2$ reforming of methane. *Appl. Catal. B Environ.* **2019**, *243*, 490–501. [CrossRef]
16. Aziz, M.A.A.; Setiabudi, H.D.; Teh, L.P.; Annuar, N.H.R.; Jalil, A.A. A review of heterogeneous catalysts for syngas production via dry reforming. *J. Taiwan Inst. Chem. Eng.* **2019**, *101*, 139–158. [CrossRef]
17. Bullock, R.M. Reaction: Earth-Abundant Metal Catalysts for Energy Conversions. *Chem* **2017**, *2*, 444–446. [CrossRef]

18. Renda, S.; Ricca, A.; Palma, V. Study of the effect of noble metal promotion in Ni-based catalyst for the Sabatier reaction. *Int. J. Hydrogen Energy* **2020**, *46*, 12117–12127. [CrossRef]

19. Wang, F.; Xu, L.; Yang, J.; Zhang, J.; Zhang, L.; Li, H.; Zhao, Y.; Li, H.X.; Wu, K.; Xu, G.Q.; et al. Enhanced catalytic performance of Ir catalysts supported on ceria-based solid solutions for methane dry reforming reaction. *Catal. Today* **2017**, *281*, 295–303. [CrossRef]

20. Andraos, S.; Abbas-Ghaleb, R.; Chlala, D.; Vita, A.; Italiano, C.; Laganà, M.; Pino, L.; Nakhl, M.; Specchia, S. Production of hydrogen by methane dry reforming over ruthenium-nickel based catalysts deposited on Al_2O_3, $MgAl_2O_4$, and YSZ. *Int. J. Hydrogen Energy* **2019**, *44*, 25706–25716. [CrossRef]

21. Chen, J.; Yao, C.; Zhao, Y.; Jia, P. Synthesis gas production from dry reforming of methane over Ce0.75Zr0.25O2-supported Ru catalysts. *Int. J. Hydrogen Energy* **2010**, *35*, 1630–1642. [CrossRef]

22. Anil, C.; Modak, J.M.; Madras, G. Syngas production via CO_2 reforming of methane over noble metal (Ru, Pt, and Pd) doped $LaAlO_3$ perovskite catalyst. *Mol. Catal.* **2020**, *484*, 110805. [CrossRef]

23. De Araujo Moreira, T.G.; de Carvalho Filho, J.F.S.; Carvalho, Y.; de Almeida, J.M.A.R.; Nothaft Romano, P.; Falabella Sousa-Aguiar, E. Highly stable low noble metal content rhodium-based catalyst for the dry reforming of methane. *Fuel* **2020**, *287*, 119536. [CrossRef]

24. Ballarini, A.D.; Virgens, C.F.; Rangel, M.C.; de Miguel, S.R.; Grau, J.M. Characterization and behaviour of Pt catalysts supported on basic materials in dry reforming of methane. *Braz. J. Chem. Eng.* **2019**, *36*, 275–284. [CrossRef]

25. Arkatova, L.A.; Kasatsky, N.G.; Maximov, Y.M.; Pakhnutov, O.V.; Shmakov, A.N. Intermetallides as the catalysts for carbon dioxide reforming of methane. *Catal. Today* **2018**, *299*, 303–316. [CrossRef]

26. Kobayashi, T.; Furuya, T.; Fujitsuka, H.; Tago, T. Synthesis of Birdcage-type zeolite encapsulating ultrafine Pt nanoparticles and its application in dry reforming of methane. *Chem. Eng. J.* **2019**, *377*, 120203. [CrossRef]

27. Gamal, A.; Eid, K.; Abdullah, A.M. Engineering of Pt-based nanostructures for efficient dry (CO_2) reforming: Strategy and mechanism for rich-hydrogen production. *Int. J. Hydrogen Energy* **2022**, *47*, 5901–5928. [CrossRef]

28. Carvalho, D.C.; De Souza, H.S.A.; Filho, J.M.; Oliveira, A.C.; Campos, A.; Milet, É.R.C.; De Sousa, F.F.; Padron-Hernandez, E. A study on the modification of mesoporous mixed oxides supports for dry reforming of methane by Pt or Ru. *Appl. Catal. A Gen.* **2014**, *473*, 132–145. [CrossRef]

29. Xie, Z.; Yan, B.; Kattel, S.; Lee, J.H.; Yao, S.; Wu, Q.; Rui, N.; Gomez, E.; Liu, Z.; Xu, W.; et al. Dry reforming of methane over CeO2-supported Pt-Co catalysts with enhanced activity. *Appl. Catal. B Environ.* **2018**, *236*, 280–293. [CrossRef]

30. Jagódka, P.; Matus, K.; Sobota, M.; Łamacz, A. Dry reforming of methane over carbon fibre-supported cezro2, ni-cezro2, pt-cezro2 and pt-ni-cezro2 catalysts. *Catalysts* **2021**, *11*, 563. [CrossRef]

31. Yang, J.; Wang, J.; Zhao, J.; Bai, Y.; Du, H.; Wang, Q.; Jiang, B.; Li, H. CO_2 conversion via dry reforming of methane on a core-shell $Ru@SiO_2$ catalyst. *J. CO2 Util.* **2022**, *57*, 101893. [CrossRef]

32. de Souza, M.G.; Melo, D.M.A.; Medeiros, R.L.B.A.; Maziviero, F.V.; Macedo, H.P.; Oliveira, Â.A.S.; Braga, R.M. NiO–$MgAl_2O_4$ systems for dry reforming of methane: Effect of the combustion synthesis route in the catalysts properties. *Mater. Chem. Phys.* **2022**, *278*, 125599. [CrossRef]

33. Azancot, L.; Blay, V.; Blay-Roger, R.; Bobadilla, L.F.; Penkova, A.; Centeno, M.A.; Odriozola, J.A. Evidence of new Ni-O-K catalytic sites with superior stability for methane dry reforming. *Appl. Catal. B Environ.* **2022**, *307*, 121148. [CrossRef]

34. Akansu, H.; Arbag, H.; Tasdemir, H.M.; Yasyerli, S.; Yasyerli, N.; Dogu, G. Nickel-based alumina supported catalysts for dry reforming of biogas in the absence and the presence of H_2S: Effect of manganese incorporation. *Catal. Today* **2022**. [CrossRef]

35. Abbas, M.; Sikander, U.; Mehran, M.T.; Kim, S.H. Exceptional stability of hydrotalcite derived spinel Mg(Ni)Al_2O_4 catalyst for dry reforming of methane. *Catal. Today* **2021**, 1–12. [CrossRef]

36. Maziviero, F.V.; Medeiros, R.L.B.A.; Melo, D.M.A.; Macedo, H.P.; Oliveira, Â.A.S.; Araújo, T.R. Synthesis of alumina by microwave-assisted combustion method using low fuel content and its use as catalytic support for dry reforming of methane. *Mater. Chem. Phys.* **2021**, *264*, 124408. [CrossRef]

37. Medeiros, R.L.B.A.; Macedo, H.P.; Melo, V.R.M.; Oliveira, Â.A.S.; Barros, J.M.F.; Melo, M.A.F.; Melo, D.M.A. Ni supported on Fe-doped $MgAl_2O_4$ for dry reforming of methane: Use of factorial design to optimize H_2 yield. *Int. J. Hydrogen Energy* **2016**, *41*, 14047–14057. [CrossRef]

38. Yao, L.; Galvez, M.E.; Hu, C.; Da Costa, P. Mo-promoted Ni/Al_2O_3 catalyst for dry reforming of methane. *Int. J. Hydrogen Energy* **2017**, *42*, 23500–23507. [CrossRef]

39. Rahbar Shamskar, F.; Meshkani, F.; Rezaei, M. Preparation and characterization of ultrasound-assisted co-precipitated nanocrys-talline La-, Ce-, Zr -promoted Ni-Al_2O_3 catalysts for dry reforming reaction. *J. CO2 Util.* **2017**, *22*, 124–134. [CrossRef]

40. Lu, Y.; Guo, D.; Ruan, Y.; Zhao, Y.; Wang, S.; Ma, X. Facile one-pot synthesis of Ni@HSS as a novel yolk-shell structure catalyst for dry reforming of methane. *J. CO2 Util.* **2018**, *24*, 190–199. [CrossRef]

41. Liu, W.; Li, L.; Zhang, X.; Wang, Z.; Wang, X.; Peng, H. Design of Ni-ZrO_2@SiO_2 catalyst with ultra-high sintering and coking resistance for dry reforming of methane to prepare syngas. *J. CO2 Util.* **2018**, *27*, 297–307. [CrossRef]

42. Peng, H.; Zhang, X.; Han, X.; You, X.; Lin, S.; Chen, H.; Liu, W.; Wang, X.; Zhang, N.; Wang, Z.; et al. Catalysts in Coronas: A Surface Spatial Confinement Strategy for High-Performance Catalysts in Methane Dry Reforming. *ACS Catal.* **2019**, *9*, 9072–9080. [CrossRef]

43. Dou, J.; Zhang, R.; Hao, X.; Bao, Z.; Wu, T.; Wang, B.; Yu, F. Sandwiched SiO$_2$@Ni@ZrO$_2$ as a coke resistant nanocatalyst for dry reforming of methane. *Appl. Catal. B Environ.* **2019**, *254*, 612–623. [CrossRef]

44. Yan, X.; Hu, T.; Liu, P.; Li, S.; Zhao, B.; Zhang, Q.; Jiao, W.; Chen, S.; Wang, P.; Lu, J.; et al. Highly efficient and stable Ni/CeO$_2$-SiO$_2$ catalyst for dry reforming of methane: Effect of interfacial structure of Ni/CeO$_2$ on SiO$_2$. *Appl. Catal. B Environ.* **2019**, *246*, 221–231. [CrossRef]

45. Sun, Y.; Zhang, G.; Liu, J.; Xu, Y.; Lv, Y. Production of syngas via CO$_2$ methane reforming process: Effect of cerium and calcium promoters on the performance of Ni-MSC catalysts. *Int. J. Hydrogen Energy* **2020**, *45*, 640–649. [CrossRef]

46. Cao, Y.; Li, H.; Zhang, J.; Shi, L.; Zhang, D. Promotional effects of rare earth elements (Sc, Y, Ce, and Pr) on NiMgAl catalysts for dry reforming of methane. *RSC Adv.* **2016**, *6*, 112215–112225. [CrossRef]

47. Sukri, M.F.F.; Khavarian, M.; Mohamed, A.R. Effect of cobalt loading on suppression of carbon formation in carbon dioxide reforming of methane over Co/MgO catalyst. *Res. Chem. Intermed.* **2018**, *44*, 2585–2605. [CrossRef]

48. Cao, A.N.T.; Pham, C.Q.; Pham, L.K.H.; Le Tri Nguyen, D.; Phuong, P.T.T.; Tran, T.T.V.; Nguyen, V.P.; Nguyen, T.B.; Van Le, Q.; Nguyen, N.A.; et al. Boosted methane dry reforming for hydrogen generation on cobalt catalyst with small cerium dosage. *Int. J. Hydrogen Energy* **2021**, 1–13. [CrossRef]

49. Bahari, M.B.; Setiabudi, H.D.; Duy Nguyen, T.; Phuong, P.T.T.; Duc Truong, Q.; Abdul Jalil, A.; Ainirazali, N.; Vo, D.V.N. Insight into the influence of rare-earth promoter (CeO$_2$, La$_2$O$_3$, Y$_2$O$_3$, and Sm$_2$O$_3$) addition toward methane dry reforming over Co/mesoporous alumina catalysts. *Chem. Eng. Sci.* **2020**, *228*, 115967. [CrossRef]

50. Tran, N.T.; Van Le, Q.; Van Cuong, N.; Nguyen, T.D.; Huy Phuc, N.H.; Phuong, P.T.T.; Monir, M.U.; Aziz, A.A.; Truong, Q.D.; Abidin, S.Z.; et al. La-doped cobalt supported on mesoporous alumina catalysts for improved methane dry reforming and coke mitigation. *J. Energy Inst.* **2020**, *93*, 1571–1580. [CrossRef]

51. El Hassan, N.; Kaydouh, M.N.; Geagea, H.; El Zein, H.; Jabbour, K.; Casale, S.; El Zakhem, H.; Massiani, P. Low temperature dry reforming of methane on rhodium and cobalt based catalysts: Active phase stabilization by confinement in mesoporous SBA-15. *Appl. Catal. A Gen.* **2016**, *520*, 114–121. [CrossRef]

52. Al-Fatesh, A.S.; Naeem, M.A.; Fakeeha, A.H.; Abasaeed, A.E. The effect of Sc promoter on the performance of Co/TiO$_2$-P25 catalyst in dry reforming of methane. *Bull. Korean Chem. Soc.* **2015**, *36*, 2081–2088. [CrossRef]

53. Kim, W.Y.; Jang, J.S.; Ra, E.C.; Kim, K.Y.; Kim, E.H.; Lee, J.S. Reduced perovskite LaNiO$_3$ catalysts modified with Co and Mn for low coke formation in dry reforming of methane. *Appl. Catal. A Gen.* **2019**, *575*, 198–203. [CrossRef]

54. Oliveira, Â.A.S.; Medeiros, R.L.B.A.; Figueredo, G.P.; Macedo, H.P.; Braga, R.M.; Maziviero, F.V.; Melo, M.A.F.; Melo, D.M.A.; Vieira, M.M. One-step synthesis of LaNiO$_3$ with chitosan for dry reforming of methane. *Int. J. Hydrogen Energy* **2018**, *43*, 9696–9704. [CrossRef]

55. Osazuwa, O.U.; Setiabudi, H.D.; Rasid, R.A.; Cheng, C.K. Syngas production via methane dry reforming: A novel application of SmCoO$_3$ perovskite catalyst. *J. Nat. Gas Sci. Eng.* **2017**, *37*, 435–448. [CrossRef]

56. Al-Doghachi, F.A.J.; Rashid, U.; Taufiq-Yap, Y.H. Investigation of Ce(III) promoter effects on the tri-metallic Pt, Pd, Ni/MgO catalyst in dry-reforming of methane. *RSC Adv.* **2016**, *6*, 10372–10384. [CrossRef]

57. Itkulova, S.S.; Valishevskiy, K.A.; Boleubayev, Y.A. Bimetallic Co-Rh Systems as a Prospective Base for Design of CH$_4$ Reforming Catalysts to Produce Syngas with a Controllable Composition. *Catalysts* **2022**, *12*, 105. [CrossRef]

58. Abd Ghani, N.A.; Azapour, A.; Syed Muhammad, S.A.F.; Mohamed Ramli, N.; Vo, D.-V.N.; Abdullah, B. Dry reforming of methane for syngas production over Ni–Co-supported Al$_2$O$_3$–MgO catalysts. *Appl. Petrochem. Res.* **2018**, *8*, 263–270. [CrossRef]

59. Tanios, C.; Gennequin, C.; Labaki, M.; Tidahy, H.L.; Aboukaïs, A.; Abi-Aad, E. Evaluation of a catalyst durability in absence and presence of toluene impurity: Case of the material Co$_2$Ni$_2$Mg$_2$Al$_2$ mixed oxide prepared by hydrotalcite route in methane dry reforming to produce energy. *Materials* **2019**, *12*, 1362. [CrossRef]

60. Movasati, A.; Alavi, S.M.; Mazloom, G. Dry reforming of methane over CeO$_2$-ZnAl$_2$O$_4$ supported Ni and Ni-Co nano-catalysts. *Fuel* **2019**, *236*, 1254–1262. [CrossRef]

61. Wysocka, I.; Hupka, J.; Rogala, A. Catalytic Activity of Nickel and Ruthenium–Nickel Catalysts Supported on SiO$_2$, ZrO$_2$, Al$_2$O$_3$, and MgAl2O4 in a Dry Reforming Process. *Catalysts* **2019**, *9*, 540. [CrossRef]

62. Singh, R.; Dhir, A.; Mohapatra, S.K.; Mahla, S.K. Dry reforming of methane using various catalysts in the process: Review. *Biomass Convers. Biorefinery* **2020**, *10*, 567–587. [CrossRef]

63. Wang, C.; Wang, Y.; Chen, M.; Liang, D.; Yang, Z.; Cheng, W.; Tang, Z. Recent advances during CH$_4$ dry reforming for syngas production: A mini review. *Int. J. Hydrogen Energy* **2020**, *46*, 5852–5874. [CrossRef]

64. Karam, L.; Armandi, M.; Casale, S.; El Khoury, V.; Bonelli, B.; Massiani, P.; El Hassan, N. Comprehensive study on the effect of magnesium loading over nickel-ordered mesoporous alumina for dry reforming of methane. *Energy Convers. Manag.* **2020**, *225*, 113470. [CrossRef]

65. Akri, M.; Zhao, S.; Li, X.; Zang, K.; Lee, A.F.; Isaacs, M.A.; Xi, W.; Gangarajula, Y.; Luo, J.; Ren, Y.; et al. Atomically dispersed nickel as coke-resistant active sites for methane dry reforming. *Nat. Commun.* **2019**, *10*, 5181. [CrossRef] [PubMed]

66. Wang, Y.; Zhao, Q.; Wang, Y.; Hu, C.; Da Costa, P. One-Step Synthesis of Highly Active and Stable Ni-ZrOxfor Dry Reforming of Methane. *Ind. Eng. Chem. Res.* **2020**, *59*, 11441–11452. [CrossRef]

67. Chein, R.Y.; Fung, W.Y. Syngas production via dry reforming of methane over CeO$_2$ modified Ni/Al$_2$O$_3$ catalysts. *Int. J. Hydrogen Energy* **2019**, *44*, 14303–14315. [CrossRef]

68. De la Cruz-Flores, V.G.; Martinez-Hernandez, A.; Gracia-Pinilla, M.A. Deactivation of Ni-SiO$_2$ catalysts that are synthetized via a modified direct synthesis method during the dry reforming of methane. *Appl. Catal. A Gen.* **2020**, *594*, 117455. [CrossRef]

69. Mahfouz, R.; Estephane, J.; Gennequin, C.; Tidahy, L.; Aouad, S.; Abi-Aad, E. CO$_2$ reforming of methane over Ni and/or Ru catalysts supported on mesoporous KIT-6: Effect of promotion with Ce. *J. Environ. Chem. Eng.* **2021**, *9*, 104662. [CrossRef]

70. Mourhly, A.; Kacimi, M.; Halim, M.; Arsalane, S. New low cost mesoporous silica (MSN) as a promising support of Ni-catalysts for high-hydrogen generation via dry reforming of methane (DRM). *Int. J. Hydrogen Energy* **2020**, *45*, 11449–11459. [CrossRef]

71. Medeiros, R.L.B.A.; Figueredo, G.P.; Macedo, H.P.; Oliveira, Â.A.S.; Rabelo-Neto, R.C.; Melo, D.M.A.; Braga, R.M.; Melo, M.A.F. One-pot microwave-assisted combustion synthesis of Ni-Al$_2$O$_3$ nanocatalysts for hydrogen production via dry reforming of methane. *Fuel* **2021**, *287*, 119511. [CrossRef]

72. Miri, S.S.; Meshkani, F.; Rastegarpanah, A.; Rezaei, M. Influence of Fe, La, Zr, Ce, and Ca on the catalytic performance and coke formation in dry reforming of methane over Ni/MgO.Al$_2$O$_3$ catalyst. *Chem. Eng. Sci.* **2022**, *250*, 116956. [CrossRef]

73. Li, S.; Gong, J. Strategies for improving the performance and stability of Ni-based catalysts for reforming reactions. *Chem. Soc. Rev.* **2014**, *43*, 7245–7256. [CrossRef] [PubMed]

74. Tian, H.; Li, X.; Zeng, L.; Gong, J. Recent Advances on the Design of Group VIII Base-Metal Catalysts with Encapsulated Structures. *ACS Catal.* **2015**, *5*, 4959–4977. [CrossRef]

75. San José-Alonso, D.; Illán-Gómez, M.J.; Román-Martínez, M.C. Low metal content Co and Ni alumina supported catalysts for the CO$_2$ reforming of methane. *Int. J. Hydrogen Energy* **2013**, *38*, 2230–2239. [CrossRef]

76. San-José-Alonso, D.; Juan-Juan, J.; Illán-Gómez, M.J.; Román-Martínez, M.C. Ni, Co and bimetallic Ni–Co catalysts for the dry reforming of methane. *Appl. Catal. A Gen.* **2009**, *371*, 54–59. [CrossRef]

77. Chen, S.; Zaffran, J.; Yang, B. Dry reforming of methane over the cobalt catalyst: Theoretical insights into the reaction kinetics and mechanism for catalyst deactivation. *Appl. Catal. B Environ.* **2020**, *270*, 118859. [CrossRef]

78. Al Abdulghani, A.J.; Park, J.H.; Kozlov, S.M.; Kang, D.C.; AlSabban, B.; Pedireddy, S.; Aguilar-Tapia, A.; Ould-Chikh, S.; Hazemann, J.L.; Basset, J.M.; et al. Methane dry reforming on supported cobalt nanoparticles promoted by boron. *J. Catal.* **2020**, *392*, 126–134. [CrossRef]

79. Ayodele, B.V.; Khan, M.R.; Cheng, C.K. Catalytic performance of ceria-supported cobalt catalyst for CO-rich hydrogen production from dry reforming of methane. *Int. J. Hydrogen Energy* **2016**, *41*, 198–207. [CrossRef]

80. Tran, N.T.; Le Minh Pham, T.; Nguyen, T.D.; Van Cuong, N.; Siang, T.J.; Phuong, P.T.T.; Jalil, A.A.; Truong, Q.D.; Abidin, S.Z.; Hagos, F.Y.; et al. Improvements in hydrogen production from methane dry reforming on filament-shaped mesoporous alumina-supported cobalt nanocatalyst. *Int. J. Hydrogen Energy* **2021**, *46*, 24781–24790. [CrossRef]

81. Levy, R.B.; Boudart, M. Platinum-Like Behavior of Tungsten Carbide in Surface Catalysis. *Science* **1973**, *181*, 547–549. [CrossRef]

82. Li, R.; Shahbazi, A.; Wang, L.; Zhang, B.; Chung, C.C.; Dayton, D.; Yan, Q. Nanostructured molybdenum carbide on biochar for CO$_2$ reforming of CH$_4$. *Fuel* **2018**, *225*, 403–410. [CrossRef]

83. Xu, Y.-T.; Xiao, X.; Ye, Z.-M.; Zhao, S.; Shen, R.; He, C.-T.; Zhang, J.-P.; Li, Y.; Chen, X.-M. Cage-Confinement Pyrolysis Route to Ultrasmall Tungsten Carbide Nanoparticles for Efficient Electrocatalytic Hydrogen Evolution. *J. Am. Chem. Soc.* **2017**, *139*, 5285–5288. [CrossRef] [PubMed]

84. Li, S.; Wang, J.; Zhang, G.; Liu, J.; Lv, Y.; Zhang, Y. Highly stable activity of cobalt based catalysts with tungsten carbide-activated carbon support for dry reforming of methane: Role of tungsten carbide. *Fuel* **2022**, *311*, 122512. [CrossRef]

85. Wang, J.; Zhang, G.; Li, G.; Liu, J.; Wang, Y.; Xu, Y.; Lyu, Y. Understanding structure-activity relationships of the highly active and stable La promoted Co/WC-AC catalyst for methane dry reforming. *Int. J. Hydrogen Energy* **2022**, *47*, 7823–7835. [CrossRef]

86. Dehimi, L.; Gaillard, M.; Virginie, M.; Erto, A.; Benguerba, Y. Investigation of dry reforming of methane over Mo-based catalysts. *Int. J. Hydrogen Energy* **2020**, *45*, 24657–24669. [CrossRef]

87. Vroulias, D.; Gkoulemani, N.; Papadopoulou, C.; Matralis, H. W–modified Ni/Al$_2$O$_3$ catalysts for the dry reforming of methane: Effect of W loading. *Catal. Today* **2020**, *355*, 704–715. [CrossRef]

88. Sasson Bitters, J.; He, T.; Nestler, E.; Senanayake, S.D.; Chen, J.G.; Zhang, C. Utilizing bimetallic catalysts to mitigate coke formation in dry reforming of methane. *J. Energy Chem.* **2022**, *68*, 124–142. [CrossRef]

89. Yusuf, M.; Farooqi, A.S.; Keong, L.K.; Hellgardt, K.; Abdullah, B. Contemporary trends in composite Ni-based catalysts for CO$_2$ reforming of methane. *Chem. Eng. Sci.* **2021**, *229*, 116072. [CrossRef]

90. Abdulrasheed, A.; Jalil, A.A.; Gambo, Y.; Ibrahim, M.; Hambali, H.U.; Shahul Hamid, M.Y. A review on catalyst development for dry reforming of methane to syngas: Recent advances. *Renew. Sustain. Energy Rev.* **2019**, *108*, 175–193. [CrossRef]

91. Pérez, J.M.M.; Lucio-Ortiz, C.J.; Rosa, J.R.; Maldonado, C.S.; De Haro Del Río, D.A.; Sandoval-Rangel, L.; Garza-Navarro, M.A.; Martínez-Vargas, D.X.; Morales-Leal, F.J. Dry Reforming of Methane for Hydrogen Production Using Bimetallic Catalysts of Pt-Fe Supported on γ-Alumina. *ChemistrySelect* **2021**, *6*, 12685–12695. [CrossRef]

92. Yentekakis, I.V.; Panagiotopoulou, P.; Artemakis, G. A review of recent efforts to promote dry reforming of methane (DRM) to syngas production via bimetallic catalyst formulations. *Appl. Catal. B Environ.* **2021**, *296*, 120210. [CrossRef]

93. Al-Fatesh, A.S.; Abu-Dahrieh, J.K.; Atia, H.; Armbruster, U.; Ibrahim, A.A.; Khan, W.U.; Abasaeed, A.E.; Fakeeha, A.H. Effect of pre-treatment and calcination temperature on Al$_2$O$_3$-ZrO$_2$ supported Ni-Co catalysts for dry reforming of methane. *Int. J. Hydrogen Energy* **2019**, *44*, 21546–21558. [CrossRef]

94. Turap, Y.; Wang, I.; Fu, T.; Wu, Y.; Wang, Y.; Wang, W. Co–Ni alloy supported on CeO$_2$ as a bimetallic catalyst for dry reforming of methane. *Int. J. Hydrogen Energy* **2020**, *45*, 6538–6548. [CrossRef]

95. Jin, F.; Fu, Y.; Kong, W.; Wang, J.; Cai, F.; Zhang, J.; Xu, J. Dry reforming of methane over trimetallic NiFeCu alloy catalysts. *Chem. Phys. Lett.* **2020**, *750*, 137491. [CrossRef]

96. Ibrahim, A.; Fakeeha, A.; Abasaeed, A.; Al-Fatesh, A. Dry Reforming of Methane Using Ni Catalyst Supported on ZrO_2: The Effect of Different Sources of Zirconia. *Catalysts* **2021**, *11*, 827. [CrossRef]

97. Bagabas, A.; Al-Fatesh, A.S.; Kasim, S.O.; Arasheed, R.; Ibrahim, A.A.; Ashamari, R.; Anojaidi, K.; Fakeeha, A.H.; Abu-Dahrieh, J.K.; Abasaeed, A.E. Optimizing MgO Content for Boosting γ-Al_2O_3-Supported Ni Catalyst in Dry Reforming of Methane. *Catalysts* **2021**, *11*, 1233. [CrossRef]

98. Gao, X.; Ge, Z.; Zhu, G.; Wang, Z.; Ashok, J.; Kawi, S. Anti-Coking and Anti-Sintering Ni/Al_2O_3 Catalysts in the Dry Reforming of Methane: Recent Progress and Prospects. *Catalysts* **2021**, *11*, 1003. [CrossRef]

99. Song, D.H.; Jung, U.H.; Kim, Y.E.; Im, H.B.; Lee, T.H.; Lee, K.B.; Koo, K.Y. Influence of Supports on the Catalytic Activity and Coke Resistance of Ni Catalyst in Dry Reforming of Methane. *Catalysts* **2022**, *12*, 216. [CrossRef]

100. Özdemir, H.; Faruk Öksüzömer, M.A.; Ali Gürkaynak, M. Preparation and characterization of Ni based catalysts for the catalytic partial oxidation of methane: Effect of support basicity on H_2/CO ratio and carbon deposition. *Int. J. Hydrogen Energy* **2010**, *35*, 12147–12160. [CrossRef]

101. Al-Fatesh, A.S.; Chaudhary, M.L.; Fakeeha, A.H.; Ibrahim, A.A.; Al-Mubaddel, F.; Kasim, S.O.; Albaqmaa, Y.A.; Bagabas, A.A.; Patel, R.; Kumar, R. Role of mixed oxides in hydrogen production through the dry reforming of methane over nickel catalysts supported on modified γ-Al_2O_3. *Processes* **2021**, *9*, 157. [CrossRef]

102. Ay, H.; Üner, D. Dry reforming of methane over CeO_2 supported Ni, Co and Ni–Co catalysts. *Appl. Catal. B Environ.* **2015**, *179*, 128–138. [CrossRef]

103. Makri, M.M.; Vasiliades, M.A.; Petallidou, K.C.; Efstathiou, A.M. Effect of support composition on the origin and reactivity of carbon formed during dry reforming of methane over 5wt% $Ni/Ce_{1-x}M_xO_{2-\delta}$ ($M=Zr^{4+}$, Pr^{3+}) catalysts. *Catal. Today* **2016**, *259*, 150–164. [CrossRef]

104. Gao, D.Z.; Strand, J.; Munde, M.S.; Shluger, A.L. Mechanisms of oxygen vacancy aggregation in SiO_2 and HfO_2. *Front. Phys.* **2019**, *7*, 43. [CrossRef]

105. Faria, E.C.; Neto, R.C.R.; Colman, R.C.; Noronha, F.B. Hydrogen production through CO_2 reforming of methane over $Ni/CeZrO_2/Al_2O_3$ catalysts. *Catal. Today* **2014**, *228*, 138–144. [CrossRef]

106. Arias-Duque, C.; Bladt, E.; Muñoz, M.A.; Hernández-Garrido, J.C.; Cauqui, M.A.; Rodríguez-Izquierdo, J.M.; Blanco, G.; Bals, S.; Calvino, J.J.; Pérez-Omil, J.A.; et al. Improving the Redox Response Stability of Ceria-Zirconia Nanocatalysts under Harsh Temperature Conditions. *Chem. Mater.* **2017**, *29*, 9340–9350. [CrossRef]

107. Rapier, R. Life Cycle Emissions of Hydrogen. Available online: https://4thgeneration.energy/life-cycles-emissions-of-hydrogen/ (accessed on 6 December 2021).

108. Tristantini, D.; Lögdberg, S.; Gevert, B.; Borg, Ø.; Holmen, A. The effect of synthesis gas composition on the Fischer–Tropsch synthesis over Co/γ-Al_2O_3 and Co–Re/γ-Al_2O_3 catalysts. *Fuel Process. Technol.* **2007**, *88*, 643–649. [CrossRef]

109. Arora, S.; Prasad, R. An overview on dry reforming of methane: Strategies to reduce carbonaceous deactivation of catalysts. *RSC Adv.* **2016**, *6*, 108668–108688. [CrossRef]

110. Akiki, E.; Akiki, D.; Italiano, C.; Vita, A.; Abbas-Ghaleb, R.; Chlala, D.; Drago Ferrante, G.; Laganà, M.; Pino, L.; Specchia, S. Production of hydrogen by methane dry reforming: A study on the effect of cerium and lanthanum on Ni/MgAl2O4 catalyst performance. *Int. J. Hydrogen Energy* **2020**, *45*, 21392–21408. [CrossRef]

111. Wurzel, T.; Malcus, S.; Mleczko, L. Reaction engineering investigations of CO_2 reforming in a fluidized-bed reactor. *Chem. Eng. Sci.* **2000**, *55*, 3955–3966. [CrossRef]

112. Mantripragada, H.C.; Veser, G. Hydrogen production via chemical looping dry reforming of methane: Process modeling and systems analysis. *AIChE J.* **2022**, e17612. [CrossRef]

113. Pajak, M.; Mozdzierz, M.; Chalusiak, M.; Kimijima, S.; Szmyd, J.S.; Brus, G. A numerical analysis of heat and mass transfer processes in a macro-patterned methane/steam reforming reactor. *Int. J. Hydrogen Energy* **2018**, *43*, 20474–20487. [CrossRef]

114. Navas-Anguita, Z.; García-Gusano, D.; Dufour, J.; Iribarren, D. Revisiting the role of steam methane reforming with CO_2 capture and storage for long-term hydrogen production. *Sci. Total Environ.* **2021**, *771*, 145432. [CrossRef] [PubMed]

115. Minh, D.P.; Siang, T.J.; Vo, D.V.N.; Phan, T.S.; Ridart, C.; Nzihou, A.; Grouset, D. *Hydrogen Production from Biogas Reforming: An Overview of Steam Reforming, Dry Reforming, Dual Reforming, and Tri-Reforming of Methane*; Elsevier Ltd.: Cambridge, MA, USA, 2018; ISBN 9780128111970.

116. Carapellucci, R.; Giordano, L. Steam, dry and autothermal methane reforming for hydrogen production: A thermodynamic equilibrium analysis. *J. Power Sources* **2020**, *469*, 228391. [CrossRef]

117. Noh, Y.S.; Lee, K.Y.; Moon, D.J. Hydrogen production by steam reforming of methane over nickel based structured catalysts supported on calcium aluminate modified SiC. *Int. J. Hydrogen Energy* **2019**, *44*, 21010–21019. [CrossRef]

118. Cho, E.; Yu, Y.J.; Kim, Y.; Phan, T.N.; Park, D.; Ko, C.H. Egg-shell-type Ni supported on MgAl2O4 pellets as catalyst for steam methane reforming: Enhanced coke-resistance and pellet stability. *Catal. Today* **2020**, *352*, 157–165. [CrossRef]

119. Kim, C.H.; Han, J.Y.; Lim, H.; Lee, K.Y.; Ryi, S.K. Methane steam reforming using a membrane reactor equipped with a Pd-based composite membrane for effective hydrogen production. *Int. J. Hydrogen Energy* **2018**, *43*, 5863–5872. [CrossRef]

120. Wang, M.; Tan, X.; Motuzas, J.; Li, J.; Liu, S. Hydrogen production by methane steam reforming using metallic nickel hollow fiber membranes. *J. Membr. Sci.* **2021**, *620*, 118909. [CrossRef]

121. Adanez, J.; Abad, A.; Garcia-Labiano, F.; Gayan, P.; de Diego, L.F. Progress in Chemical-Looping Combustion and Reforming technologies. *Prog. Energy Combust. Sci.* **2012**, *38*, 215–282. [CrossRef]

122. Medeiros, R.L.B.A.; Melo, V.R.M.; Melo, D.M.A.; Macedo, H.P.; Moure, G.T.; Adánez-Rubio, I.; Melo, M.A.F.; Adánez, J. Double perovskite (La$_{2-x}$Ca-Ba$_x$)NiO$_4$ oxygen carriers for chemical looping reforming applications. *Int. J. Hydrogen Energy* **2019**, *45*, 1681–1696. [CrossRef]

123. Moghtaderi, B. Review of the recent chemical looping process developments for novel energy and fuel applications. *Energy Fuels* **2012**, *26*, 15–40. [CrossRef]

124. Barros do Nascimento, R.A.; Pimenta de Macedo, H.; Melo, D.M.A.; Santiago, R.C.; Rodrigues de Araújo, T.; Medeiros, R.L.B.A.; Adánez, J. Structure and Reactivity of Brazilian Iron Ores as Low-Cost Oxygen Carriers for Chemical Looping Combustion. *Ind. Eng. Chem. Res.* **2022**, 2469–2482. [CrossRef]

125. Zhu, M.; Song, Y.; Chen, S.; Li, M.; Zhang, L.; Xiang, W. Chemical looping dry reforming of methane with hydrogen generation on Fe$_2$O$_3$/Al$_2$O$_3$ oxygen carrier. *Chem. Eng. J.* **2019**, *368*, 812–823. [CrossRef]

126. Chein, R.Y.; Hsu, W.H. Thermodynamic analysis of syngas production via chemical looping dry reforming of methane. *Energy* **2019**, *180*, 535–547. [CrossRef]

127. Löfberg, A.; Kane, T.; Guerrero-Caballero, J.; Jalowiecki-Duhamel, L. Chemical looping dry reforming of methane: Toward shale-gas and biogas valorization. *Chem. Eng. Process. Process Intensif.* **2017**, *122*, 523–529. [CrossRef]

128. Li, D.; Xu, R.; Gu, Z.; Zhu, X.; Qing, S.; Li, K. Chemical-Looping Conversion of Methane: A Review. *Energy Technol.* **2020**, *8*, 1900925. [CrossRef]

129. Guerrero-Caballero, J.; Kane, T.; Haidar, N.; Jalowiecki-Duhamel, L.; Löfberg, A. Ni, Co, Fe supported on Ceria and Zr doped Ceria as oxygen carriers for chemical looping dry reforming of methane. *Catal. Today* **2019**, *333*, 251–258. [CrossRef]

130. Kim, Y.; Lim, H.S.; Lee, M.; Lee, J.W. Ni-Fe-Al mixed oxide for combined dry reforming and decomposition of methane with CO$_2$ utilization. *Catal. Today* **2021**, *368*, 86–95. [CrossRef]

131. Sastre, D.; Galván, C.Á.; Pizarro, P.; Coronado, J.M. Enhanced performance of CH$_4$ dry reforming over La$_{0.9}$Sr$_{0.1}$FeO$_3$/YSZ under chemical looping conditions. *Fuel* **2022**, *309*, 122122. [CrossRef]

132. Soria, M.A.; Mateos-Pedrero, C.; Guerrero-Ruiz, A.; Rodríguez-Ramos, I. Thermodynamic and experimental study of combined dry and steam reforming of methane on Ru/ZrO$_2$-La$_2$O$_3$ catalyst at low temperature. *Int. J. Hydrogen Energy* **2011**, *36*, 15212–15220. [CrossRef]

133. Park, N.; Park, M.J.; Baek, S.C.; Ha, K.S.; Lee, Y.J.; Kwak, G.; Park, H.G.; Jun, K.W. Modeling and optimization of the mixed reforming of methane: Maximizing CO$_2$ utilization for non-equilibrated reaction. *Fuel* **2014**, *115*, 357–365. [CrossRef]

134. Jokar, S.M.; Parvasi, P.; Basile, A. The evaluation of methane mixed reforming reaction in an industrial membrane reformer for hydrogen production. *Int. J. Hydrogen Energy* **2018**, *43*, 15321–15329. [CrossRef]

135. Jabbour, K. Tuning combined steam and dry reforming of methane for "metgas" production: A thermodynamic approach and state-of-the-art catalysts. *J. Energy Chem.* **2020**, *48*, 54–91. [CrossRef]

136. Dan, M.; Mihet, M.; Lazar, M.D. Hydrogen and/or syngas production by combined steam and dry reforming of methane on nickel catalysts. *Int. J. Hydrogen Energy* **2020**, *45*, 26254–26264. [CrossRef]

137. Batebi, D.; Abedini, R.; Mosayebi, A. Combined steam and CO$_2$ reforming of methane (CSCRM) over Ni–Pd/Al$_2$O$_3$ catalyst for syngas formation. *Int. J. Hydrogen Energy* **2020**, *45*, 14293–14310. [CrossRef]

138. Sengodan, S.; Lan, R.; Humphreys, J.; Du, D.; Xu, W.; Wang, H.; Tao, S. Advances in reforming and partial oxidation of hydrocarbons for hydrogen production and fuel cell applications. *Renew. Sustain. Energy Rev.* **2018**, *82*, 761–780. [CrossRef]

139. Alvarez-Galvan, C.; Melian, M.; Ruiz-Matas, L.; Eslava, J.L.; Navarro, R.M.; Ahmadi, M.; Cuenya, B.R.; Fierro, J.L.G. Partial oxidation of methane to syngas over nickel-based catalysts: Influence of support type, addition of rhodium, and preparation method. *Front. Chem.* **2019**, *7*, 104. [CrossRef] [PubMed]

140. Roseno, K.T.C.; Schmal, M.; Brackmann, R.; Alves, R.M.B.; Giudici, R. Partial oxidation of methane on neodymium and lanthanum chromate based perovskites for hydrogen production. *Int. J. Hydrogen Energy* **2019**, *44*, 8166–8177. [CrossRef]

141. Christian Enger, B.; Lødeng, R.; Holmen, A. A review of catalytic partial oxidation of methane to synthesis gas with emphasis on reaction mechanisms over transition metal catalysts. *Appl. Catal. A Gen.* **2008**, *346*, 1–27. [CrossRef]

142. Ding, C.; Wang, J.; Guo, S.; Ma, Z.; Li, Y.; Ma, L.; Zhang, K. Abundant hydrogen production over well dispersed nickel nanoparticles confined in mesoporous metal oxides in partial oxidation of methane. *Int. J. Hydrogen Energy* **2019**, *44*, 30171–30184. [CrossRef]

143. Zhao, X.; Joseph, B.; Kuhn, J.; Ozcan, S. Biogas Reforming to Syngas: A Review. *iScience* **2020**, *23*, 101082. [CrossRef]

144. Zhang, Y.; Zhang, S.; Gossage, J.L.; Lou, H.H.; Benson, T.J. Thermodynamic analyses of tri-reforming reactions to produce syngas. *Energy Fuels* **2014**, *28*, 2717–2726. [CrossRef]

145. Pham Minh, D.; Pham Xuan, H.; Siang, T.J.; N.Vo, D.-V. A review on the impact of operating conditions, catalyst deactivation and regeneration in tri-reforming of methane. *Appl. Catal. A Gen.* **2021**, *621*, 118202. [CrossRef]

146. MacIel, L.J.L.; De Souza, A.E.M.; Cavalcanti-Filho, V.O.; Knoechelmann, A.; De Abreu, C.A.M. Kinetic evaluation of the tri-reforming process of methane for syngas production. *React. Kinet. Mech. Catal.* **2010**, *101*, 407–416. [CrossRef]

147. Majewski, A.J.; Wood, J. Tri-reforming of methane over Ni@SiO$_2$ catalyst. *Int. J. Hydrogen Energy* **2014**, *39*, 12578–12585. [CrossRef]

148. Pino, L.; Vita, A.; Cipitì, F.; Laganà, M.; Recupero, V. Hydrogen production by methane tri-reforming process over Ni-ceria catalysts: Effect of La-doping. *Appl. Catal. B Environ.* **2011**, *104*, 64–73. [CrossRef]

149. García-Vargas, J.M.; Valverde, J.L.; Dorado, F.; Sánchez, P. Influence of the support on the catalytic behaviour of Ni catalysts for the dry reforming reaction and the tri-reforming process. *J. Mol. Catal. A Chem.* **2014**, *395*, 108–116. [CrossRef]

150. Chutichairattanaphum, N.; Narataruksa, P.; Pana-Suppamassadu, K.; Tungkamani, S.; Prapainainar, C.; Chotiwan, S.; Wattanathana, W. Effects of Raschig Ring Packing Patterns on Pressure Drop, Heat Transfer, Methane Conversion, and Coke Deposition on a Semi-pilot-scale Packed Bed Reformer. *Chem. Biochem. Eng. Q.* **2019**, *33*, 191–211. [CrossRef]

151. Kahle, L.C.S.; Roussière, T.; Maier, L.; Herrera Delgado, K.; Wasserschaff, G.; Schunk, S.A.; Deutschmann, O. Methane dry reforming at high temperature and elevated pressure: Impact of gas-phase reactions. *Ind. Eng. Chem. Res.* **2013**, *52*, 11920–11930. [CrossRef]

152. Wang, H.; Duan, X.; Liu, X.; Ye, G.; Gu, X.; Zhu, K.; Zhou, X.; Yuan, W. Influence of tubular reactor structure and operating conditions on dry reforming of methane. *Chem. Eng. Res. Des.* **2018**, *139*, 39–51. [CrossRef]

153. Aouad, S.; Labaki, M.; Ojala, S.; Seelam, P.; Turpeinen, E.; Gennequin, C.; Estephane, J.; Aad, E.A. A Review on the Dry Reforming Processes for Hydrogen Production: Catalytic Materials and Technologies. In *Catalytic Materials for Hydrogen Production and Electro-Oxidation Reactions*; Bentham Books: Sharjah, United Arab Emirates, 2018; pp. 60–128.

154. Caloric GmbH Carbon Monoxide Generation Plants and Production Technologies. Available online: https://www.caloric.com/en/product/carbon-monoxide-generation-plants/ (accessed on 9 February 2022).

155. Teuner, S.C.; Neumann, P.; Von Linde, F. The Calcor standard and Calcor economy processes. *Oil Gas Eur. Mag.* **2001**, *27*, 44–46.

156. Van Diepen, A.E.; Kapteijn, F.; Makkee, M.; Moulijn, J.A. Contribution of Catalysis Towards the Reduction of Atmospheric Air Pollution: CO_2, CFCs, N_2O, Ozone. In *Environmental Catalysis*; Janssen, F.J.J., van Santen, R.A., Eds.; Imperial College Press: London, UK, 1999; pp. 219–256.

157. Mortensen, P.M.; Dybkjær, I. Industrial scale experience on steam reforming of CO_2-rich gas. *Appl. Catal. A Gen.* **2015**, *495*, 141–151. [CrossRef]

158. Wittich, K.; Krämer, M.; Bottke, N.; Schunk, S.A. Catalytic Dry Reforming of Methane: Insights from Model Systems. *ChemCatChem* **2020**, *12*, 2130–2147. [CrossRef]

159. Midrex Technologies Inc. MIDREX Plants. Available online: https://www.midrex.com/about-midrex/midrex-plants-map/ (accessed on 10 February 2022).

160. Sarkar, S.; Bhattacharya, R.; Roy, G.G.; Sen, P.K. Modeling MIDREX Based Process Configurations for Energy and Emission Analysis. *Steel Res. Int.* **2018**, *89*, 1700248. [CrossRef]

161. Farhadi, F.; Motemed Hashemi, M.Y.; Bahrami Babaheidari, M. Modelling and simulation of syngas unit in large scale direct reduction plant. *Ironmak. Steelmak.* **2003**, *30*, 18–24. [CrossRef]

162. Linde Engineering. Smaller Carbon Footprint. Higher Process Efficiency. Available online: https://www.engineering.linde.com/dryref (accessed on 9 February 2022).

163. Bartesch, T.; Wawrzinek, K.; Behrens, A.; Peschel, A. DRYREF & SYNSPIRE Innovation for HyCO Applications. In Proceedings of the Global Syngas Technologies Conference, Virtual Conference, 20–21, 27–28 October 2020.

164. York, A.P.E.; Xiao, T.; Green, M.L.H.; Claridge, J.B. Methane Oxyforming for Synthesis Gas Production. *Catal. Rev.* **2007**, *49*, 511–560. [CrossRef]

165. Shah, Y.T.; Gardner, T.H. Dry Reforming of Hydrocarbon Feedstocks. *Catal. Rev.* **2014**, *56*, 476–536. [CrossRef]

166. Shang, Z.; Li, S.; Li, L.; Liu, G.; Liang, X. Highly active and stable alumina supported nickel nanoparticle catalysts for dry reforming of methane. *Appl. Catal. B Environ.* **2017**, *201*, 302–309. [CrossRef]

167. Rezaei, E.; Dzuryk, S. Techno-economic comparison of reverse water gas shift reaction to steam and dry methane reforming reactions for syngas production. *Chem. Eng. Res. Des.* **2019**, *144*, 354–369. [CrossRef]

168. Osaki, T.; Horiuchi, T.; Suzuki, K.; Mori, T. Suppression of carbon deposition in CO_2-reforming of methane on metal sulfide catalysts. *Catal. Lett.* **1995**, *35*, 39–43. [CrossRef]

169. Midrex Technologies Inc. About Midrex. Available online: https://www.midrex.com/about-midrex/ (accessed on 10 February 2022).

170. Linde Engineering. Technologies that Do More with Less. Available online: https://www.linde-engineering.com/en/about-linde-engineering/success-stories/technologies-more-with-less.html (accessed on 9 February 2022).

171. Kelling, R.; Eigenberger, G.; Nieken, U. Ceramic counterflow reactor for autothermal dry reforming at high temperatures. *Catal. Today* **2016**, *273*, 196–204. [CrossRef]